NASA TM X-581

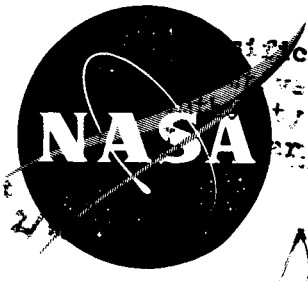

TECHNICAL MEMORANDUM

X-581

THE SUBSONIC AERODYNAMIC CHARACTERISTICS OF SOME BLUNT DELTA CONFIGURATIONS WITH 75° SWEEPBACK

By George G. Edwards and Howard F. Savage

Ames Research Center
Moffett Field, Calif.

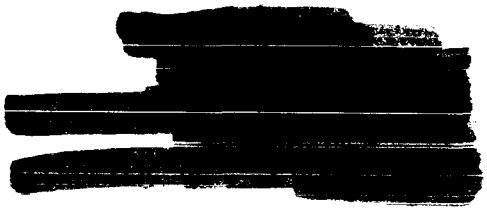

NATIONAL AERONAUTICS AND SPACE ADMINISTRATION

WASHINGTON

October 1961

NATIONAL AERONAUTICS AND SPACE ADMINISTRATION

TECHNICAL MEMORANDUM X-581

THE SUBSONIC AERODYNAMIC CHARACTERISTICS OF SOME BLUNT DELTA CONFIGURATIONS WITH 75° SWEEPBACK*

By George G. Edwards and Howard F. Savage

SUMMARY

A wind-tunnel investigation has been conducted at subsonic speeds to study the effects on performance and stability of modifications to a delta plan-form wing with 75° sweepback. Six-component force and moment data, together with base pressure, are presented for a number of delta wings all having the same plan form but with a variety of thickness distributions, leading-edge shapes, and base areas. Also investigated were the effects of a small and a large fuselage, fuselage boattailing, tip-mounted vertical surfaces, and elevon controls. The effects of variation of Reynolds numbers from 2.2 million to 22 million at a constant Mach number of 0.25 and the effects of variation of Mach number from 0.25 to 0.90 at a constant Reynolds number of 2.2 million are included for selected configurations.

INTRODUCTION

One class of atmosphere entry vehicles potentially capable of more or less conventional landing is characterized by highly swept delta plan forms. To ease the heating problem and to provide adequate internal volume, the designer is often led to consider relatively thick wings with blunt leading edges and large fuselages. Questions arise as to how these departures from more conventional supersonic aircraft may affect the performance and stability at subsonic speeds. To provide some answers to these questions, a number of highly swept delta plan-form models were investigated in the Ames 12-Foot Pressure Wind Tunnel. Shapes investigated ranged from essentially a flat-plate wing to complete configurations with large leading-edge radii and large internal volume. The model shapes were selected to provide information on aerodynamic effects resulting from changes in leading-edge shape, longitudinal section profile, and base area, and the effects of adding a fuselage, vertical surfaces, and elevon controls.

*Title, Unclassified

Six-component force and moment data, together with base pressures, were obtained for a range of angles of attack and sideslip. Most of the tests were performed at a Mach number of 0.25, although in a few instances, tests were extended to a Mach number of 0.90. The effects of varying Reynolds number from 2.2 million to 22 million at a Mach number of 0.25 were studied for selected configurations as were the effects of leading-edge roughness. The results are summarized herein without analysis.

NOTATION

The results are referred to the body axes except for the lift and drag coefficients which are referred to the stability axes. The moment center was located on the longitudinal axis at 46.7 percent of the root chord of the blunt-nosed plan form (see figs. 1 through 5). The coefficients and symbols are defined as follows:

a minor axis of base ellipse

b span or major axis of base ellipse

c root chord of blunt-nosed plan form

C_D drag coefficient, $\frac{\text{drag}}{qS}$

$C_{D_{base}}$ base drag coefficient, $C_p \frac{S_b}{S} \cos \alpha$ (C_p obtained from pressure measurement with single pressure tube at the rear of the balance cavity adjacent to the sting)

C_L lift coefficient, $\frac{\text{lift}}{qS}$

C_l rolling-moment coefficient, $\frac{\text{rolling moment}}{qSb}$

C_m pitching-moment coefficient, $\frac{\text{pitching moment}}{qSc}$

C_n yawing-moment coefficient, $\frac{\text{yawing moment}}{qSb}$

C_p base-pressure coefficient, $\frac{p_b - p}{q}$

C_Y side-force coefficient, $\frac{\text{side force}}{qS}$

L.E.	leading edge
$\frac{L}{D}$	lift-drag ratio
M	free-stream Mach number
p	free-stream static pressure
p_b	static pressure at the base of models
q	free-stream dynamic pressure
R	Reynolds number based on c and free-stream conditions
S	plan-form area (not including area of elevons)
S_b	base area
x,y,z	orthogonal coordinates with origin at the nose of the model
α	angle of attack, referenced to the longitudinal axis of the wing, deg
β	angle of sideslip, deg
δ_h	deflection of horizontal control surface (see fig. 5(a)), deg
δ_r	angle of the vertical surfaces to a plane through the leading edges (see fig. 5(a)), deg

MODELS

The geometric properties of the models are given in the sketches and photographs of figures 1 through 5 and in table I. The flat-plate models, referred to herein as models 1 and 2 (fig. 1), were fabricated of aluminum and incorporated a steel housing for the strain-gage balance. Models 3, 4, 5, and 6 (figs. 2 through 5) were constructed of wood fitted around a steel sleeve which housed the balance. The models were painted with lacquer and hand rubbed with No. 400 sandpaper to a smooth finish.

The models were mounted in the test section of the wind tunnel on a sting-type support with a 2.50-inch diameter, six-component strain-gage balance for measuring forces and moments. For most of the tests, the base pressure was measured with a single tube at the rear of the balance cavity adjacent to the sting. Model 3 had additional static-pressure

orifices distributed over the base to obtain an average base pressure for comparison with the pressure measured with the single tube at the sting.

All models except model 1 had the same basic plan form with 75° sweepback and a parabolic nose which was tangent to the straight leading edges at one-third of the length. The aspect ratio was 1.17 except when elevons or vertical surfaces were added. The plan form of model 1 differed only in that the nose was pointed, resulting in an aspect ratio of 1.07. Additional information on the models is contained in the following paragraphs.

Models 1 and 2

Models 1 and 2 were flat-plate models differing only in plan form as mentioned above and as shown in figure 1. Each was provided with two types of leading and trailing edges. In one case, the leading and trailing edges of the 1/2-inch plate were beveled (fig. 1) and in the other, the leading edge was round and the trailing edge was blunt. The balance was housed in a minimum size, faired enclosure on the top surface (fig. 1).

Models 3A and 3B

The proportions of model 3A were identical to those of model 3 of reference 1. All sections perpendicular to the longitudinal center line of model 3A were ellipses with a ratio of major axis to minor axis of 3. The model was basically an elliptic cone but with parabolic nose sections in plan and side views. As shown in figure 2, the parabolas were tangent to the straight-line portions of the leading edge at one-third the length of the model.

Model 3B was a modification of model 3A obtained by removing the top part of the model to leave a flat surface 1.50 inches above and parallel to the center line (see fig. 2).

Models 4A, 4B, 4C, and 4D

Model 4A differed from model 3A in that the nose had much larger effective leading-edge radii although it had the same 3 to 1 elliptical base. As shown in figure 3, the center-line profile had an elliptical nose with straight-line fairing aft to the base. All sections perpendicular to the longitudinal center line were ellipses with the minor axis determined by the center-line profile.

Models 4B, 4C, and 4D were modifications of model 4A in which the minor axis of the base ellipse was successively reduced but the nose was not changed (see fig. 3). The ratios of major axis to minor axis of the bases for models 4B, 4C, and 4D were 4, 5, and 6, respectively, and the base areas are given in table II.

Model 5

As illustrated in figure 4(a), the center-line profile was a modified NACA four-digit airfoil of about 17-percent thickness ratio with a blunt trailing edge. All sections normal to the plane of symmetry were ellipses, the major axes being specified by the plan form and the minor axes by the coordinates of the center-line profile. The base was an ellipse (b/a = 6) with area equal to 15.3 percent of the plan-form area. Since all sections normal to the plane of symmetry were ellipses, the surfaces of the basic model were analytic and free of discontinuities. This wing was tested alone and with either of two sizes of fuselage mounted on the top surface (fig. 4). The large fuselage increased the base area to 19.7 percent of the plan-form area and the small fuselage increased it to 16.3 percent.

Model 6

The wing of model 6 was a modification of model 5 (cf. figs. 4 and 5) to reduce the base area, in which material was removed from the rear half of the upper surface, with no change in the lower surface or the forward part of the upper surface. The modification produced fair airfoil sections at lateral stations from either of the two fuselages to 0.8 of the semi-span. Along the leading edge near the tip where the radius normal to the leading edge of model 5 was less than 0.8 inch, the radius for the modified model (model 6) was increased to a constant value of about 0.8 inch. This was done in consideration of the leading-edge heating problem on re-entry vehicles. The upper surface coordinates of model 6 at several longitudinal stations behind the symmetrical nose are given in table III.

Model 6 could not be tested without a fuselage since the strain-gage balance was covered by the fuselage. The fuselages used with model 5 were adapted to model 6 by extending them toward the horizontal plane to meet the re-countoured upper surface. At one point in the investigation, an arc with a 30-inch radius was used to boattail the large fuselage so that the base area of the fuselage was reduced to that of the small fuselage (see fig. 5(a)). With either the small fuselage or the boattailed large fuselage, model 6 had a base area of 9.9 percent of the plan-form area, and with the large unboattailed fuselage the base area was 14 percent.

Elevon control surfaces were attached to the trailing edge and had a total area equal to 5.6 percent of the plan-form area exclusive of control surfaces. The control surfaces were set at angles $\delta_h = +5^\circ$, -8°, and -18° (see fig. 5(a)). The tips of the wing of model 6 were clipped slightly to accommodate the vertical surfaces as shown in figures 5(a) and 5(c). The vertical surfaces could be installed either normal to the chord plane ($\delta_r = 90^\circ$) or canted outward 20° ($\delta_r = 110^\circ$). These surfaces had a total area of 22.7 percent of the clipped plan-form area.

TESTS

At a Mach number of 0.25 and a Reynolds number of 4.4 million, based on c, six-component force and moment measurements were made for all models through a range of angles of attack with zero sideslip. Measurements were also made through a range of angles of attack at a nearly constant angle of sideslip of 9° and through a range of angles of sideslip at a nearly constant angle of attack of 9°. The effects of Reynolds number on the longitudinal characteristics of models 2, 3A, 4A, 5, and 6 were investigated at Reynolds numbers up to 22 million with a constant Mach number of 0.25. For the same group of models, the effects of Mach number to a maximum Mach number of 0.90 were obtained through a range of angles of attack at zero sideslip. The effects of roughness in the form of No. 100 carborundum grit on the leading edges of models 3A, 4A, and 6 were studied at Mach number 0.25.

CORRECTIONS TO DATA

The measured angles of attack and of sideslip have been corrected for static deflection of the balance and sting. The induced effects of the tunnel walls resulting from lift on the model were calculated by the method of reference 2 and since the influence on angle of attack and drag coefficient was small, no corrections were applied.

The constriction effects due to the tunnel walls were calculated by the method of reference 3 and corrections were applied to the Mach number and the dynamic pressure. The magnitude of these corrections for a configuration involving the largest corrections is illustrated by the following table:

Corrected Mach number	Uncorrected Mach number	$\frac{q_{uncorrected}}{q_{corrected}}$
0.250	0.249	0.998
.600	.598	.995
.900	.881	.978

The chord force used to compute C_D and C_L was that measured by the strain-gage balance and thus includes the effects of base pressure and sting interference.

PRESENTATION OF DATA

The results of this investigation are presented in figures 6 through 38, grouped as follows according to the type of model configuration under study:

Flat-plate models (Models 1 and 2)	Figures 6 through 10
A blunt elliptical cone and one modification (Models 3A and 3B)	Figures 11 through 15
Thick delta wings (Models 4A, 4B, 4C, and 4D)	Figures 16 through 23
Thick delta re-entry configurations (Models 5 and 6)	Figures 24 through 38

In general, each group of figures contains, in addition to the basic forces and moments, some information on the effects of Reynolds number, Mach number, and surface roughness. Lift-drag ratios of models in the first three groups are compared in figure 22. Measured values of $(L/D)_{max}$ and base drag coefficient, $(C_{D_{base}})_{\alpha=0}$, for these models are correlated as functions of base-area ratio, S_b/S, in figure 23. Note that with the exception of one of the flat-plate models and of the re-entry configuration with tip-mounted vertical surfaces, all models had the same plan form.

The lateral and directional characteristics are presented both as functions of angle of attack and angle of sideslip. The coefficients presented as functions of angle of attack are divided by β since the angle of sideslip could not be held constant but varied from about 8.2° to 9°.

SUMMARY OF RESULTS

At low speeds, the delta plan-form wings without fuselage or vertical surfaces provided essentially linear lift and pitching-moment characteristics with a variety of thickness distributions, leading-edge shapes, and base areas (figs. 6 through 21).

The wing thickness changes had only small effects on the pitching-moment characteristics. However, the thickened wings had a considerably lower lift-curve slope and higher drag due to lift than did the flat-plate wings (figs. 6, 7, 11, 16, and 18). The base drag, and as a result, the total drag, decreased almost linearly with base area and the base area was the primary factor affecting the maximum lift-drag ratio (fig. 23). A delta wing having a symmetrical NACA four-digit center-line profile with blunt base was modified by removal of material from the top surface well aft of the leading edge (cf. figs. 4 and 5). The modification would not change the aerodynamic heating characteristics of the bottom surface nor of the leading edges. The resulting reduction in base area and camber effect produced significant increases in lift-drag ratio. However, camber effects provided somewhat more negative pitching moment at zero lift (figs. 24 and 25).

Clipping the wing tips and adding vertical surfaces improved the lift-drag ratio (figs. 24, 25, 27, and 28). Tilt-out of the vertical surfaces produced similar effects (figs. 27 and 28).

A comparison of two configurations with large and small fuselages showed that by boattailing the large fuselage so that its base area equalled that of the small fuselage, the lift-drag ratios of the two configurations could be made comparable (cf. figs. 24 and 25). A problem with fuselage boattailing in the manner applied is the rearward shift in the center of pressure which produces a more negative pitching moment at zero lift (fig. 30).

A re-entry configuration consisting of a thick delta wing with modified upper surface, a fuselage, vertical surfaces, and elevons could be trimmed at low speeds with a lift-drag ratio of 5 at a lift coefficient of 0.3 (fig. 29). The static longitudinal stability margin was 6 percent of the center-line length with the center of gravity at 0.467 of the length.

The results for the complete configuration showed a nearly linear variation of pitching moment with lift to at least a lift coefficient of 0.4 (angle of attack of 10° to 12°) at Mach numbers to 0.90. However, a sudden forward shift in center of pressure occurred at some higher lift coefficient at Mach numbers of 0.80 and above (fig. 32).

The directional stability was maintained at a high level with the vertical fins for angles of attack up to the maximum tested (24°). The dihedral effect was large and increased with increasing angle of attack up to an angle of attack of about 14° (fig. 38).

Ames Research Center
National Aeronautics and Space Administration
Moffett Field, Calif., Aug. 8, 1961

REFERENCES

1. McDevitt, John B., and Rakich, John V.: The Aerodynamic Characteristics of Several Thick Delta Wings at Mach Numbers to 6 and Angles of Attack to 50°. NASA TM X-162, 1960.

2. Glauert, H.: The Elements of Aerofoil and Airscrew Theory. The Macmillan Company, 1943.

3. Herriot, John G.: Blockage Corrections for Three-Dimensional-Flow Closed-Throat Wind Tunnels, With Consideration of the Effect of Compressibility. NACA Rep. 995, 1950. (Supersedes NACA RM A7B28)

TABLE I.- GEOMETRIC PROPERTIES OF THE MODELS

Sweepback of leading edge, deg	75.0
Aspect ratio	
Model 1	1.07
Models 2, 3, 4, 5, and 6 (without elevons or vertical surfaces)	1.17
Model 6 (with vertical surfaces, without elevons)	0.86
Plan-form area, sq ft	
Model 1	3.270
Models 2, 3, 4, 5, and 6 (without elevons or vertical surfaces)	3.000
Model 6 (with elevons, without vertical surfaces)	3.167
Model 6 (without elevons, with vertical surfaces)	2.910
Model 6 (with elevons and vertical surfaces)	3.077
Span, ft	
All models except model 6 with vertical surfaces	1.87
Model 6 with vertical surfaces	1.58
Length, ft	
Model 1, sharp leading edge	3.50
Model 1, round leading edge	3.44
Models 2, 3, 4, 5, and 6 (without elevons)	2.62
Base area, sq ft	
Models 1 and 2 (sharp trailing edge, balance housing only)	0.091
Models 1 and 2 (blunt trailing edge)	0.134
Model 3A	0.918
Model 3B	0.689
Model 4A	0.918
Model 4B	0.689
Model 4C	0.551
Model 4D	0.459
Model 5	0.459
Model 5 with small fuselage	0.502
Model 5 with large fuselage	0.590
Model 6 with small fuselage, no elevons or vertical surfaces	0.296
Model 6 with large fuselage, no elevons or vertical surfaces	0.421
Model 6 with large fuselage boattailed, no elevons or vertical surfaces	0.296
Model 6 with small fuselage and elevons	0.255
Model 6 with small fuselage and vertical surfaces but no elevons	0.276
Model 6 with small fuselage, vertical surfaces, and elevons	0.235

TABLE II.- RATIO OF BASE AREA TO PLAN-FORM AREA OF THE MODELS

Model 1, sharp leading and trailing edges	0.028
Model 1, round leading edge, blunt trailing edge	0.041
Model 2, sharp leading and trailing edges	0.030
Model 2, round leading edge, blunt trailing edge	0.045
Model 3A	0.306
Model 3B	0.230
Model 4A	0.306
Model 4B	0.230
Model 4C	0.184
Model 4D	0.153
Model 5	0.153
Model 5 with small fuselage	0.167
Model 5 with large fuselage	0.197
Model 6 with small fuselage, no elevons or vertical surfaces	0.099
Model 6 with large fuselage, no elevons or vertical surfaces	0.140
Model 6 with large fuselage and elevons, no vertical surfaces	0.122
Model 6 with large fuselage boattailed, no elevons or vertical surfaces	0.099
Model 6 with small fuselage and elevons, or large fuselage boattailed and elevons	0.081
Model 6 with small fuselage and vertical surfaces but no elevons	0.095
Model 6 with small fuselage, vertical surfaces, and elevons	0.076

TABLE III.- UPPER SURFACE COORDINATES OF MODEL 6

x = 8		x = 12		x = 16		x = 20		x = 24	
±y	z	±y	z	±y	z	±y	z	±y	z
2.45	2.06	2.50	2.03	2.00	1.82	2.00	1.40	2.00	0.60
2.95	1.89	3.00	1.92	2.50	1.72	2.50	1.30	2.50	.50
3.19	1.80	3.50	1.80	3.00	1.62	3.00	1.18	3.00	.44
3.44	1.72	4.00	1.67	3.50	1.52	3.50	1.08	3.50	.40
3.68	1.62	4.52	1.50	4.00	1.42	4.00	.98	4.00	.35
3.93	1.49	4.82	1.39	4.50	1.31	4.50	.88	4.50	.31
4.17	1.34	5.12	1.27	5.00	1.19	5.00	.80	5.00	.28
4.42	1.14	5.42	1.09	6.00	.94	5.50	.76	5.50	.25
4.54	.99	5.57	.97	6.50	.78	6.00	.74	6.00	.26
4.66	.81	5.72	.82	6.75	.65	6.50	.75	6.50	.30
4.78	.58	5.87	.59	7.00	.38	7.00	.79	7.00	.39
4.86	.37	5.96	.38	7.10	0			7.50	.53
4.91	0	6.02	0					8.00	.70
						7.37	Center of 0.8 radius circle z = 0	8.20	.78
								8.44	Center of 0.8 radius circle z = .02
								9.24	.02

x = 28		x = 31.46	
±y	z	±y	z
2.00	-0.30	2.00	-0.95
2.50	-.30	2.50	-.93
3.00	-.30	3.00	-.90
3.50	-.30	3.50	-.88
4.00	-.30	4.00	-.85
4.50	-.30	4.50	-.82
5.00	-.30	5.00	-.78
5.50	-.28	5.50	-.74
6.00	-.25	6.00	-.69
6.50	-.20	6.50	-.63
7.00	- 12	7.00	-.57
7.50	-.03	7.50	-.49
8.00	.13	8.00	-.40
8.50	.38	8.50	-.30
9.00	.68	9.00	-.10
9.51	Center of 0.8 radius circle z = .08	9.25	.05
		10.44	Center of 0.8 radius circle z = .22
10.31	.08	11.24	.22

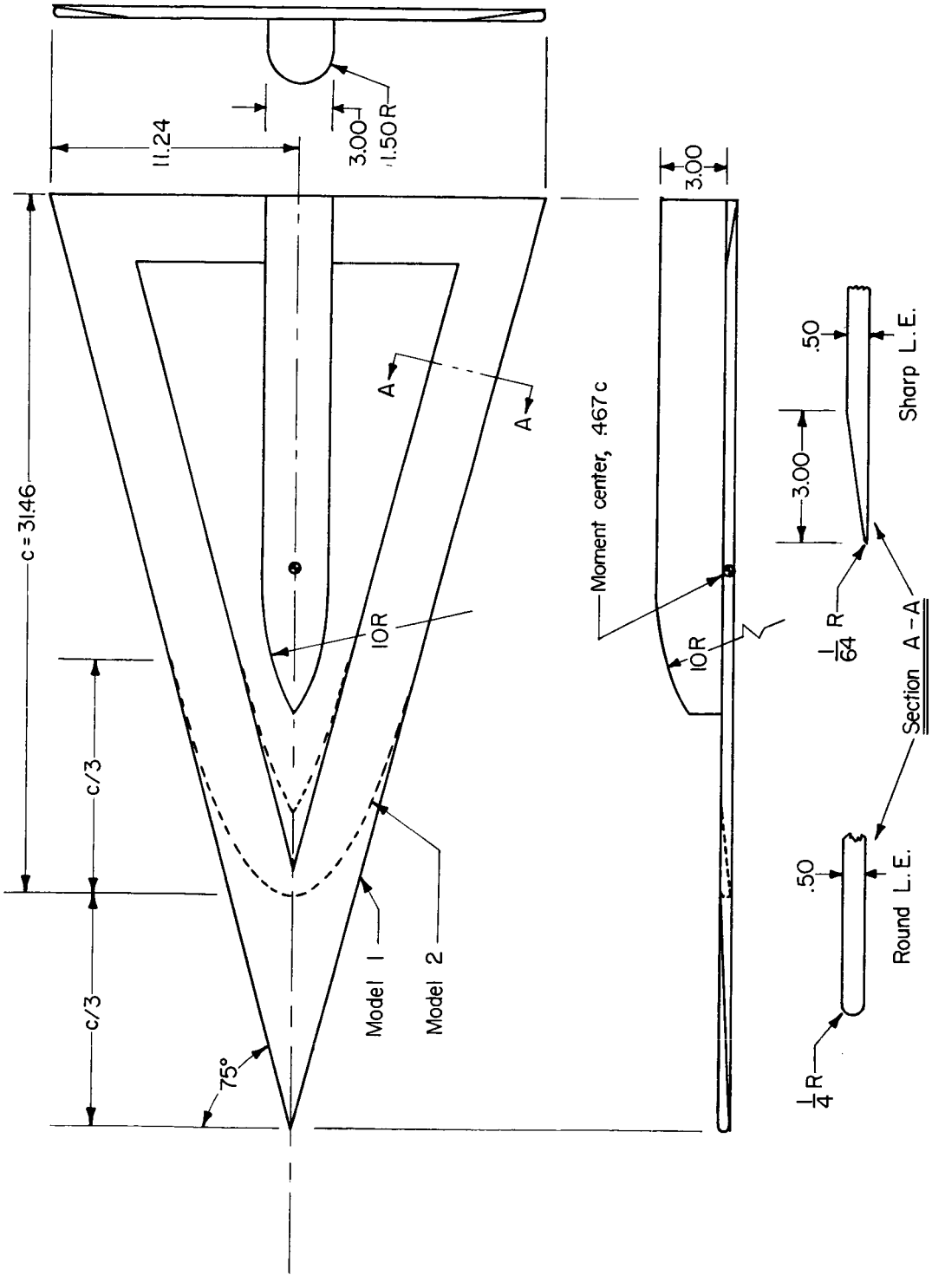

Figure 1.- Geometry of models 1 and 2; all dimensions in inches.

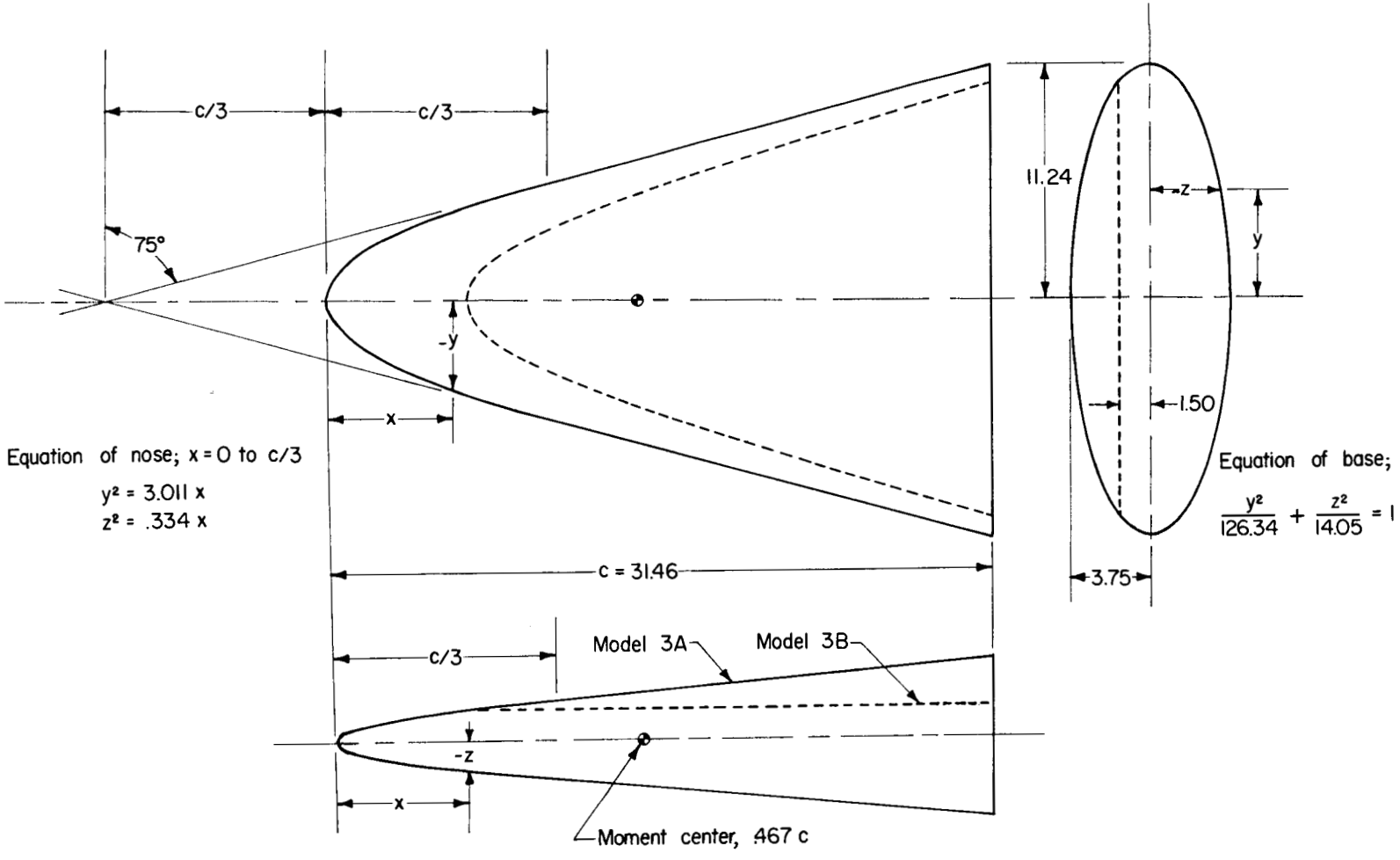

Figure 2.- Geometry of models 3A and 3B; all dimensions in inches.

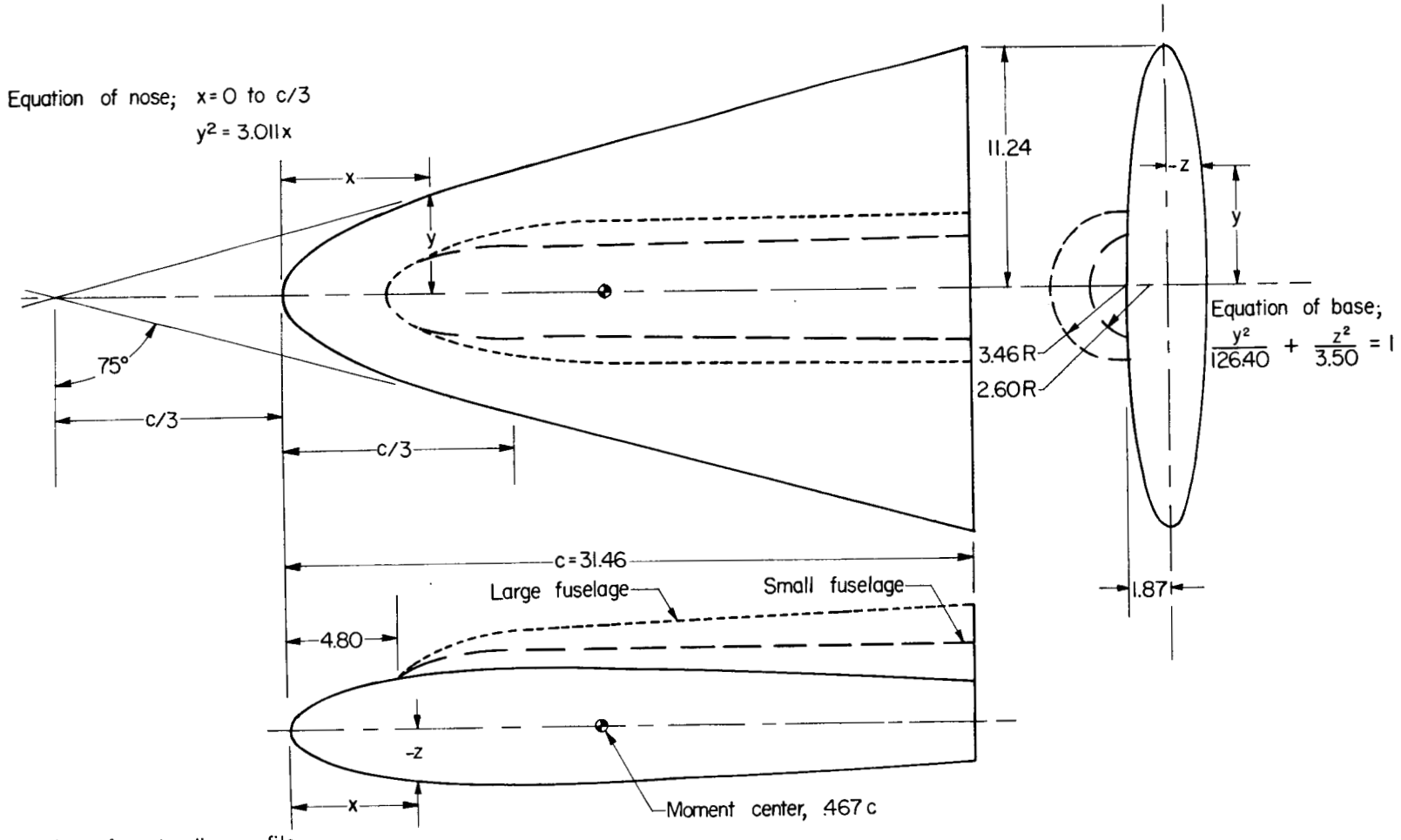

(a) Details of model 5.

Figure 4.- Geometry of model 5; all dimensions in inches.

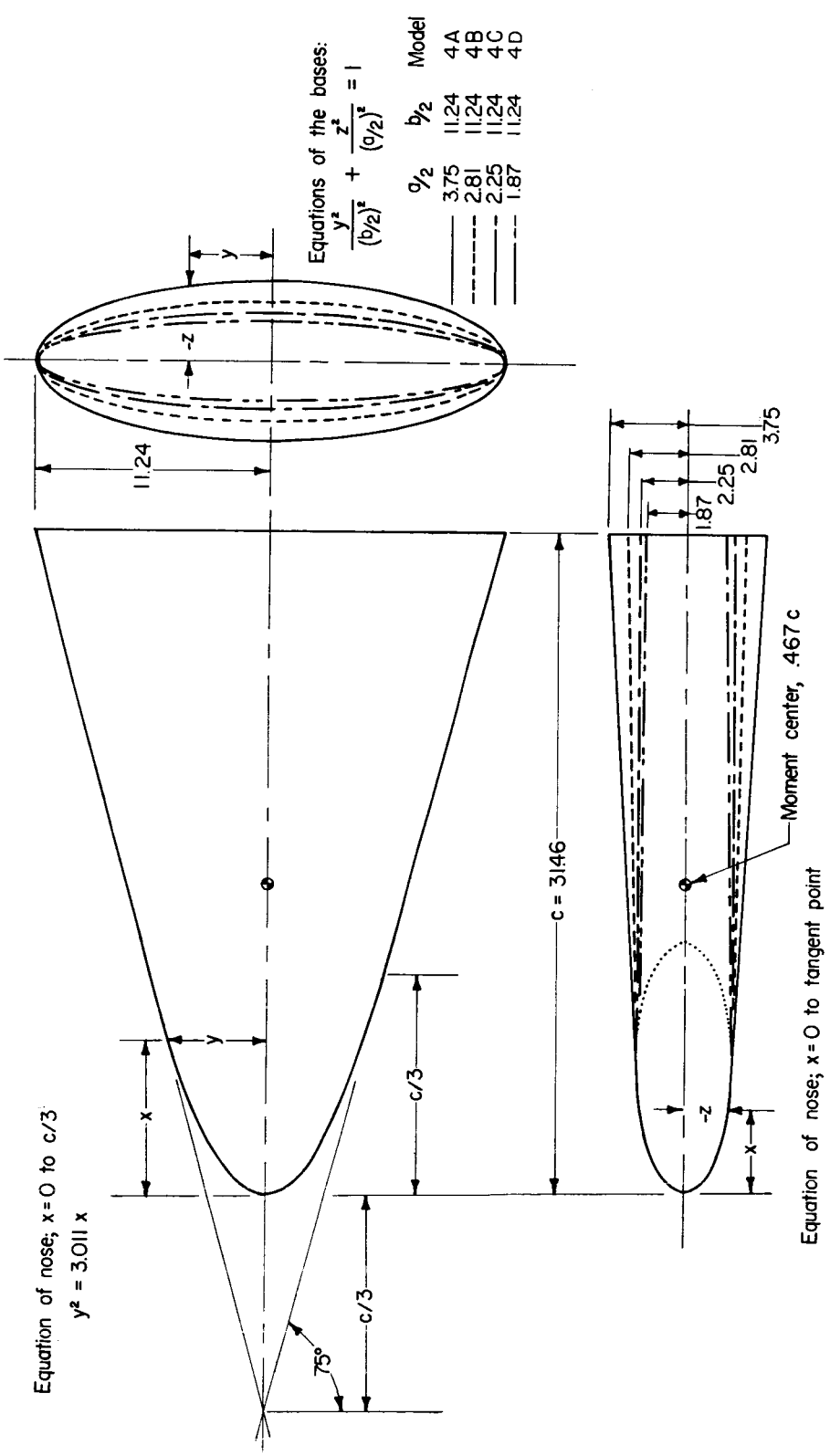

Figure 3.- Geometry of models 4A, 4B, 4C, and 4D; all dimensions in inches.

(b) Model 5 without fuselage. A-24920

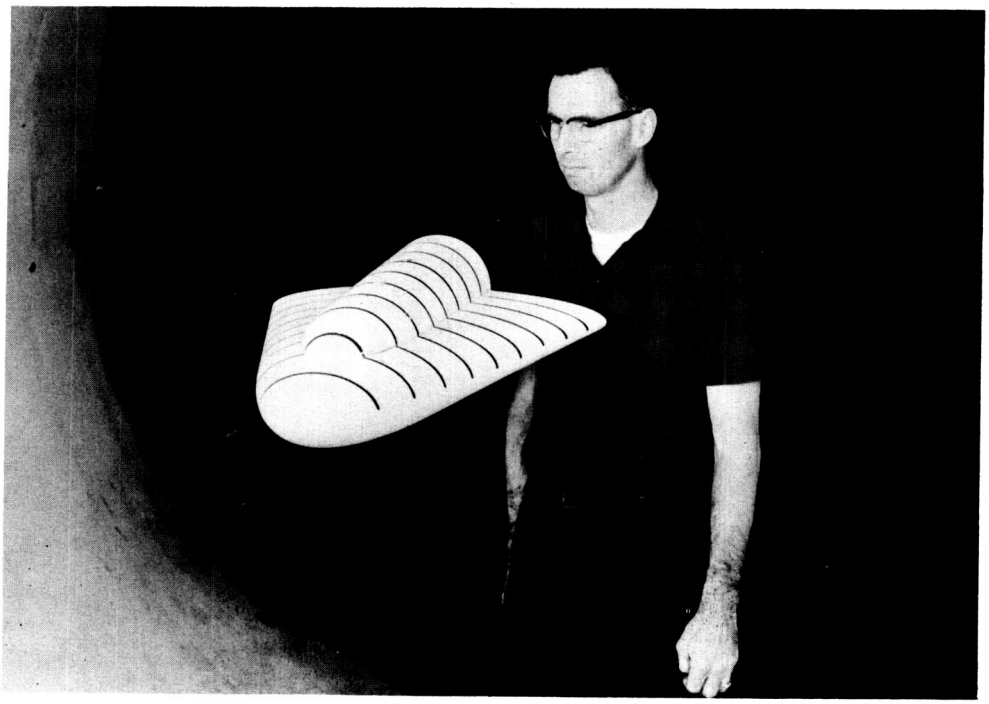

(c) Model 5 with large fuselage. A-24914

Figure 4.- Concluded.

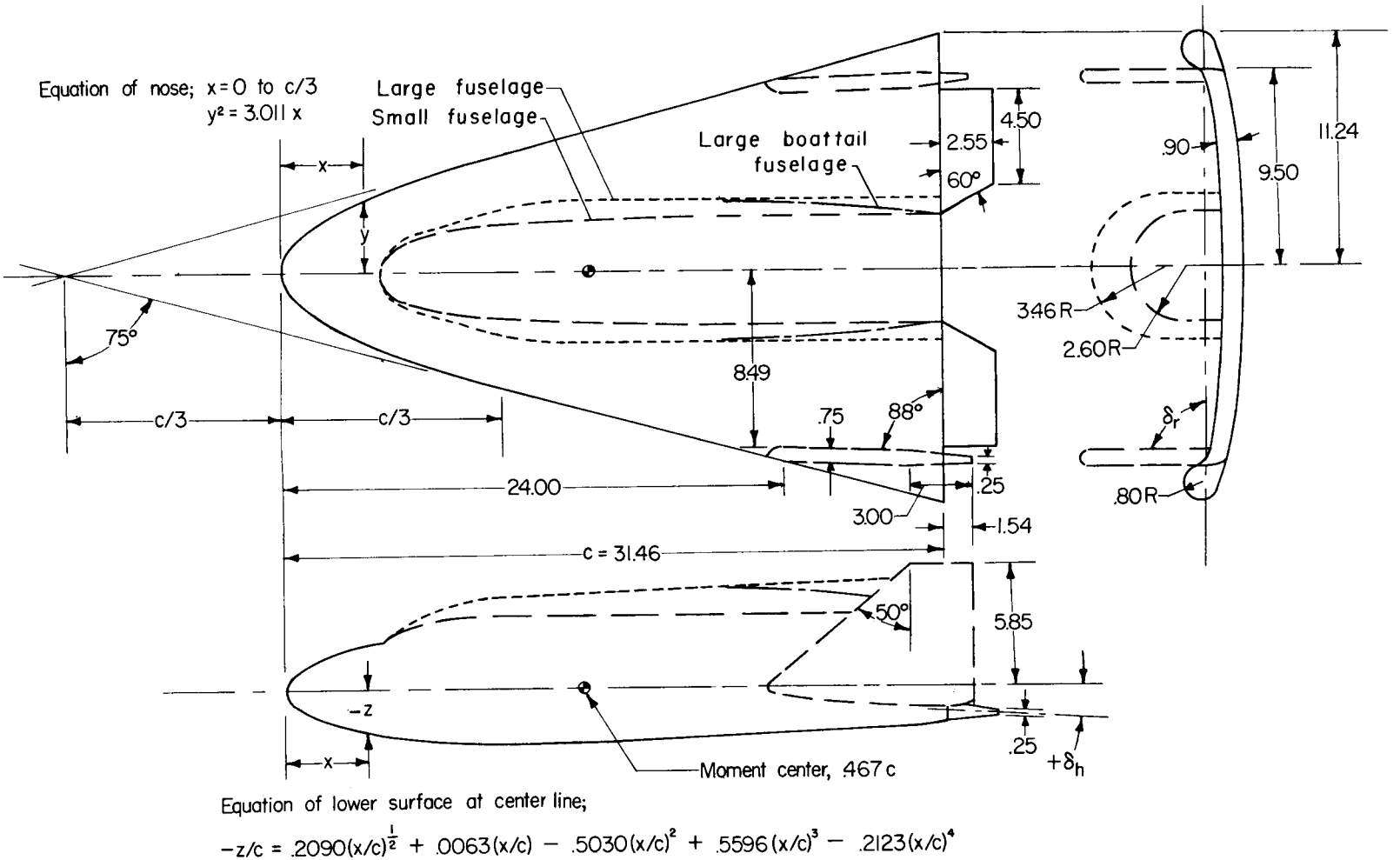

(a) Details of model 6.

Figure 5.- Geometry of model 6; all dimensions in inches.

(b) Model 6 with large fuselage. A-24921

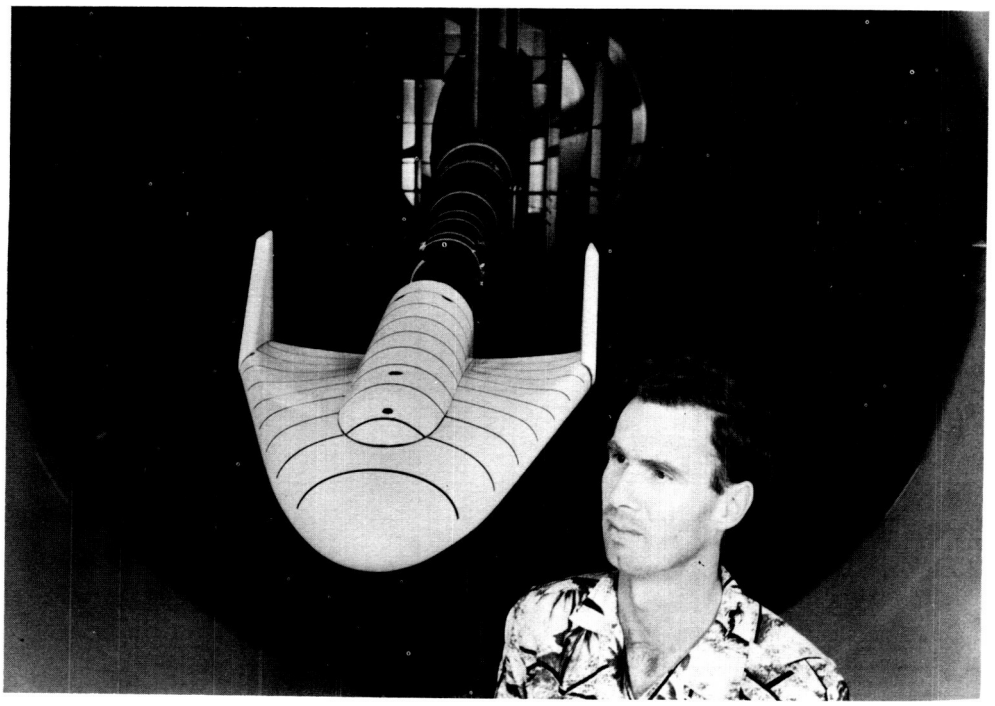

A-25567

(c) Model 6 with small fuselage and vertical surfaces; $\delta_r = 90^\circ$.

Figure 5.- Concluded.

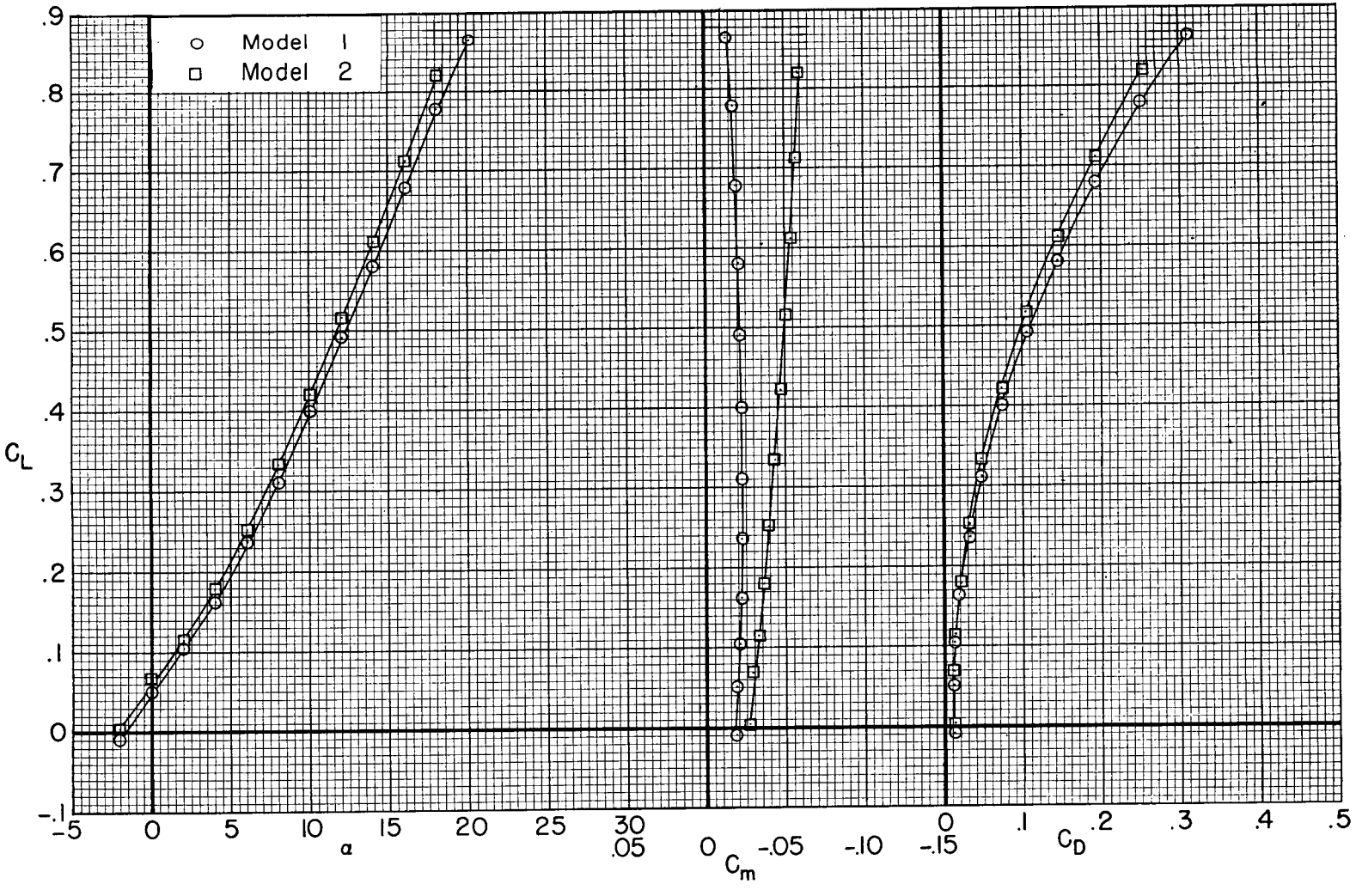

Figure 6.- The effects of plan form on the lift, drag, and pitching-moment characteristics of flat-plate models with sharp leading edges; M = 0.25, R = 4.4 million, $\beta = 0^{\circ}$.

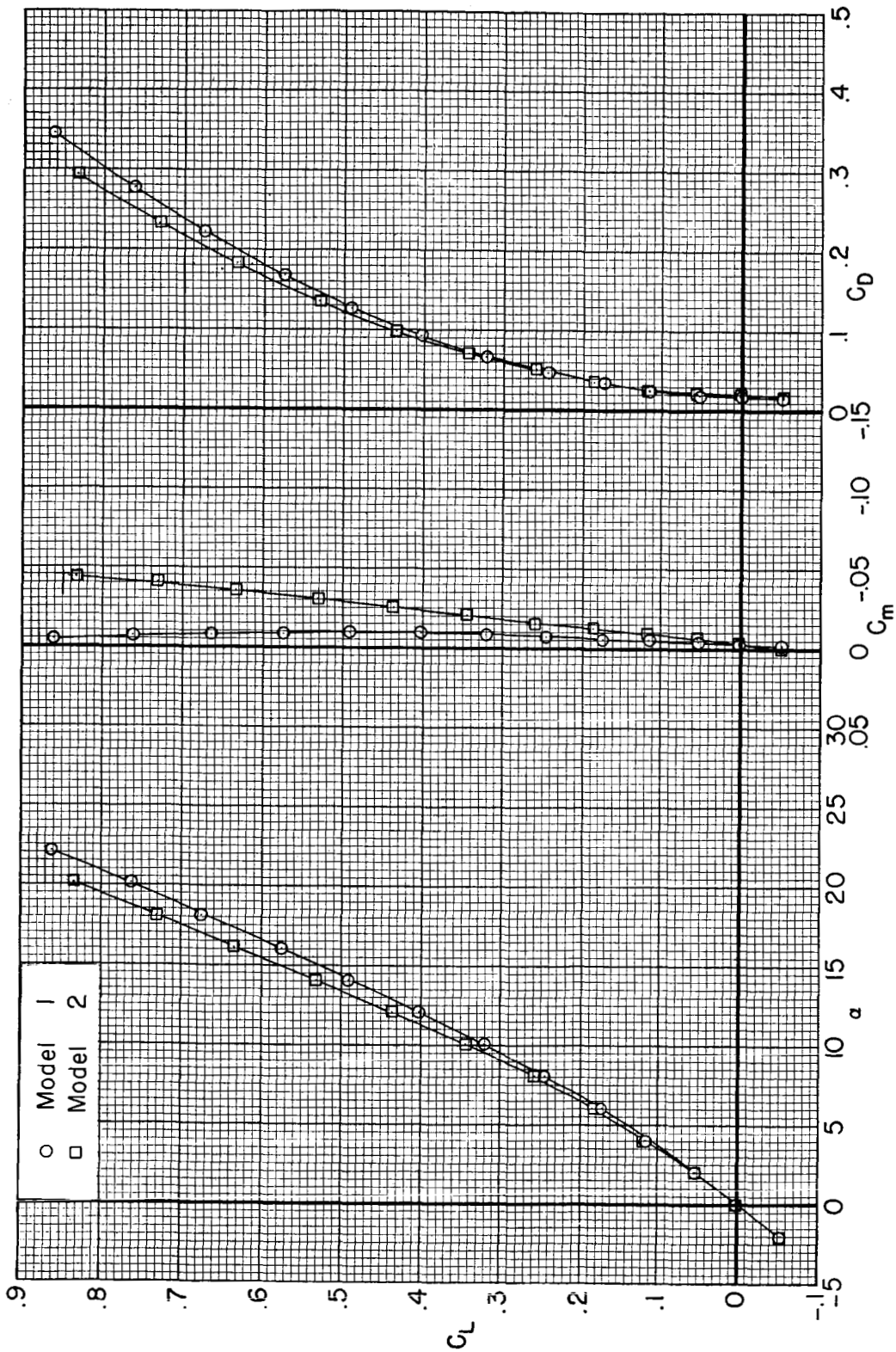

Figure 7.- The effects of plan form on the lift, drag, and pitching-moment characteristics of flat-plate models with round leading edges; M = 0.25, R = 4.4 million, $\beta = 0^{\circ}$.

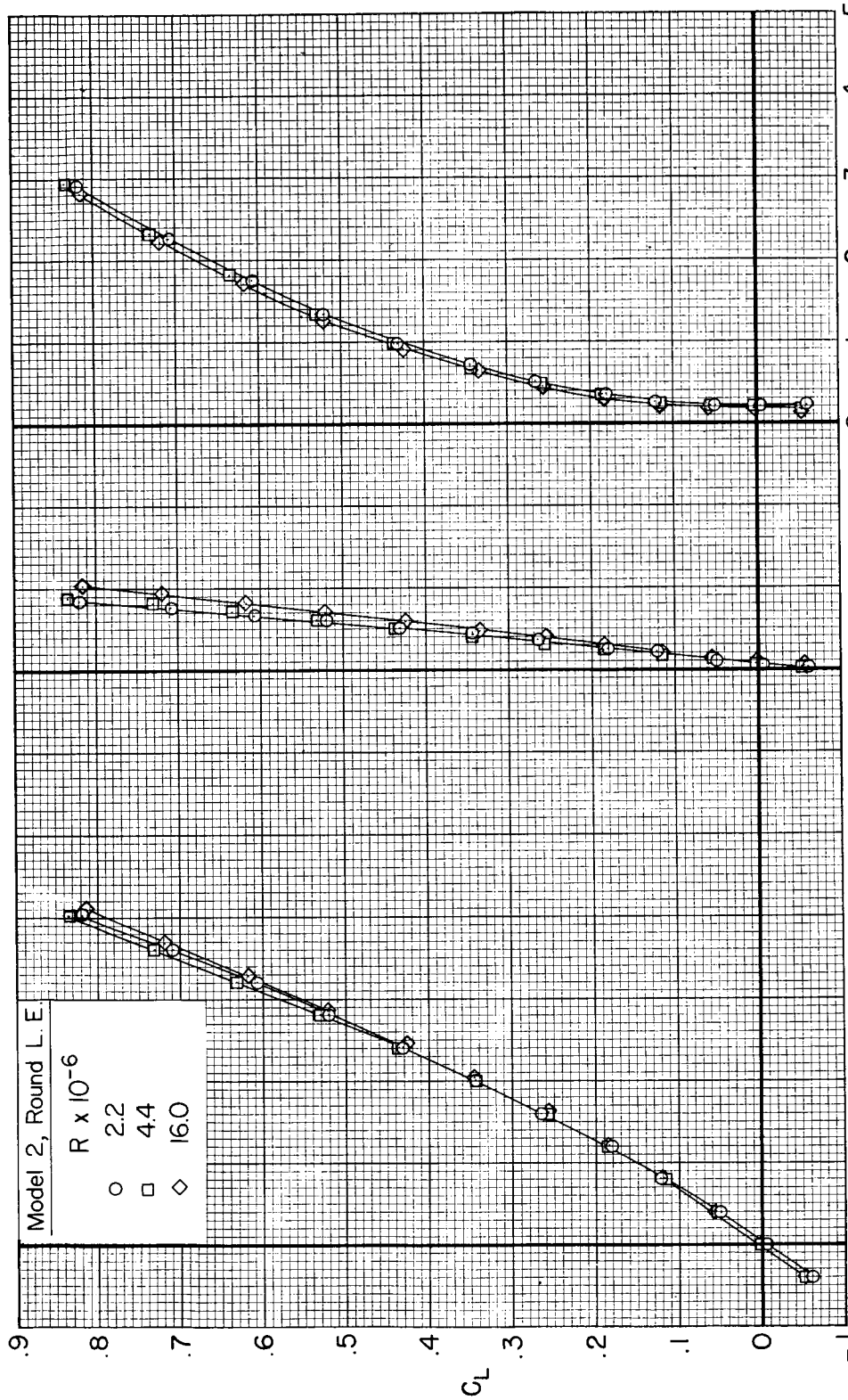

Figure 8.- The effects of Reynolds number on the longitudinal aerodynamic characteristics of flat-plate model 2 with round leading edges; M = 0.25, $\beta = 0^{\circ}$.

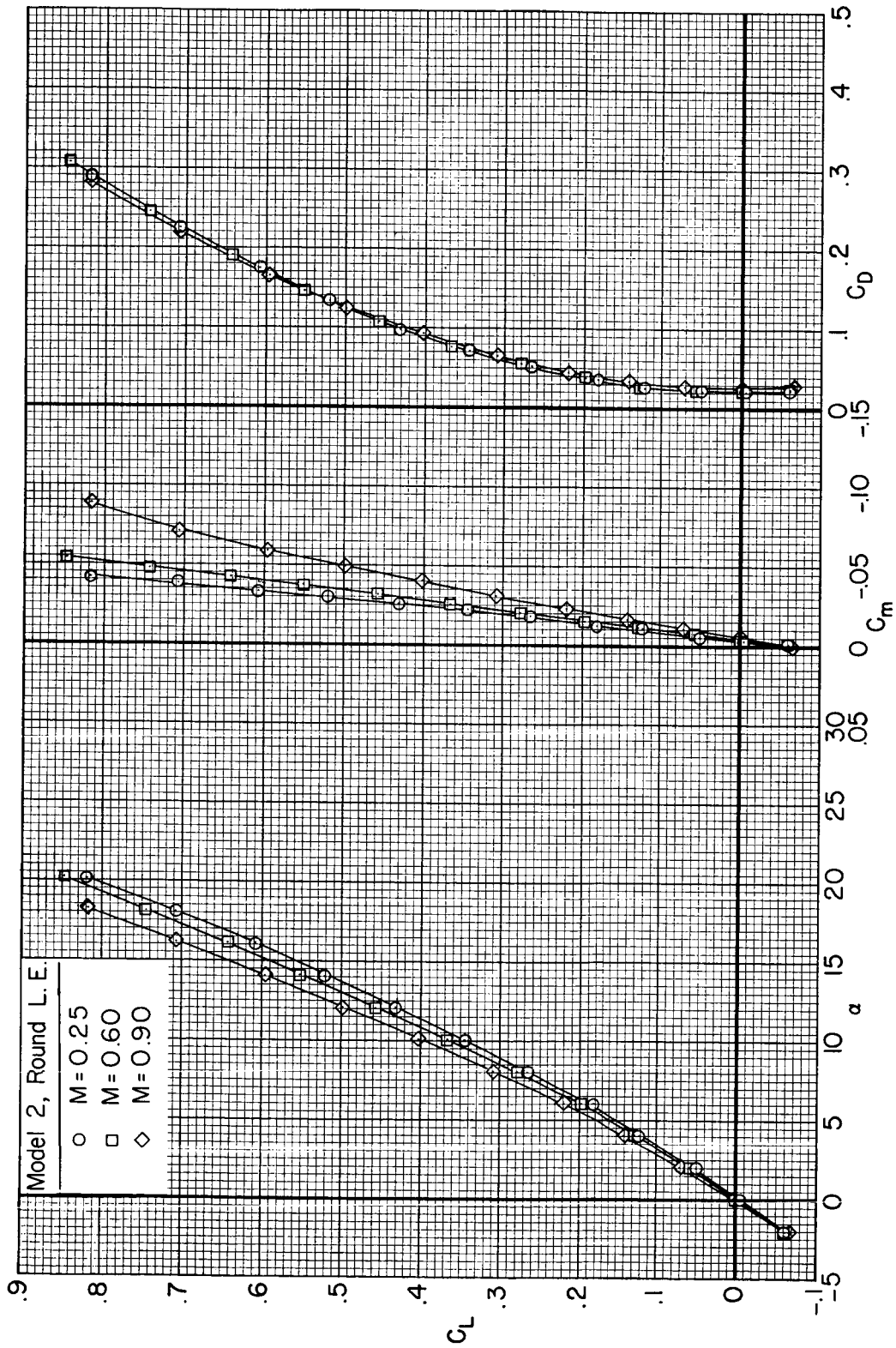

Figure 9.- The effects of Mach number on the longitudinal aerodynamic characteristics of flat-plate model 2 with round leading edge; R = 2.2 million, $\beta = 0^{\circ}$.

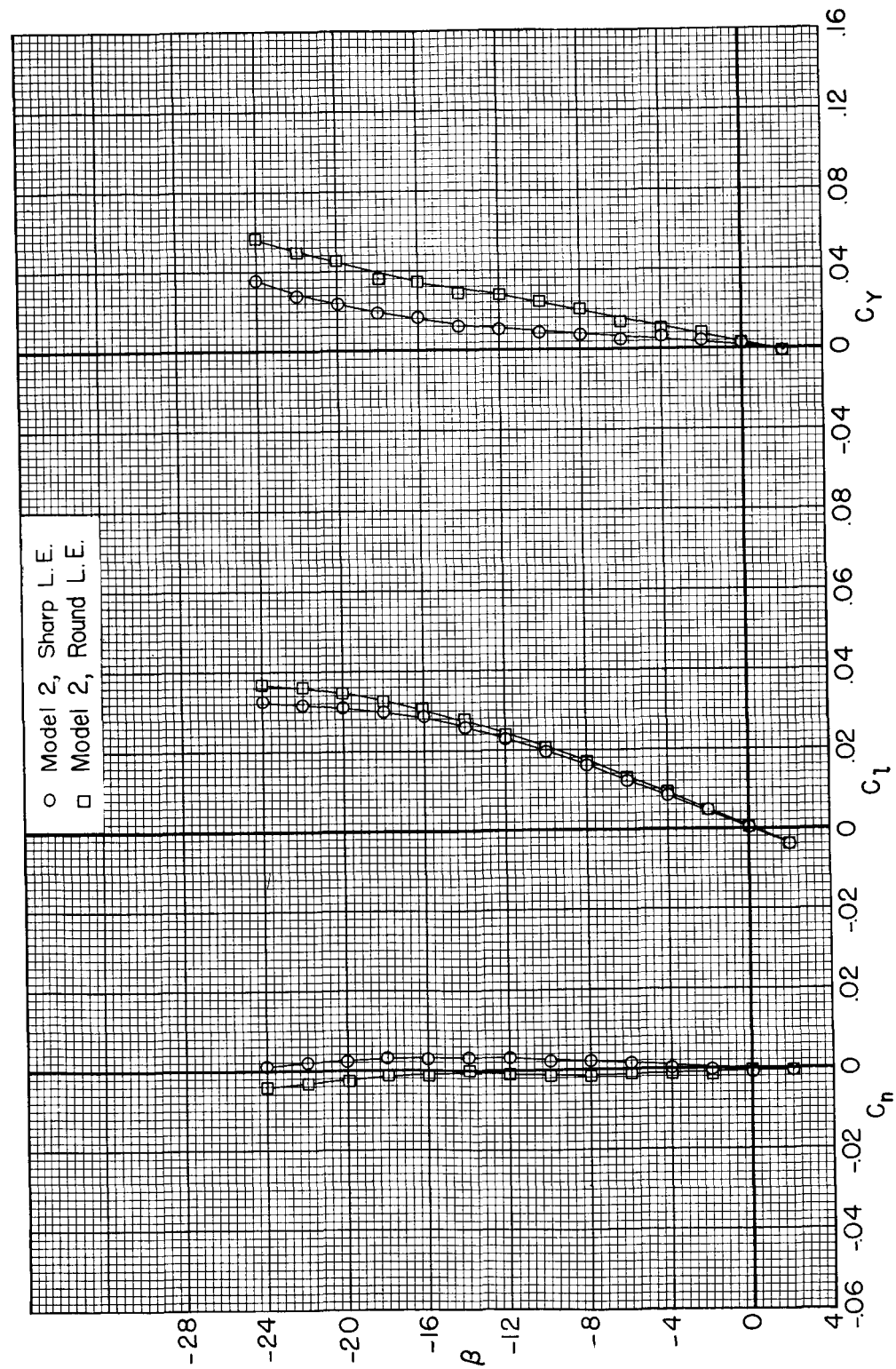

(a) β variable, α = ~9°.

Figure 10.- The lateral and directional characteristics of model 2 with sharp and with round leading edges; M = 0.25, R = 4.4 million.

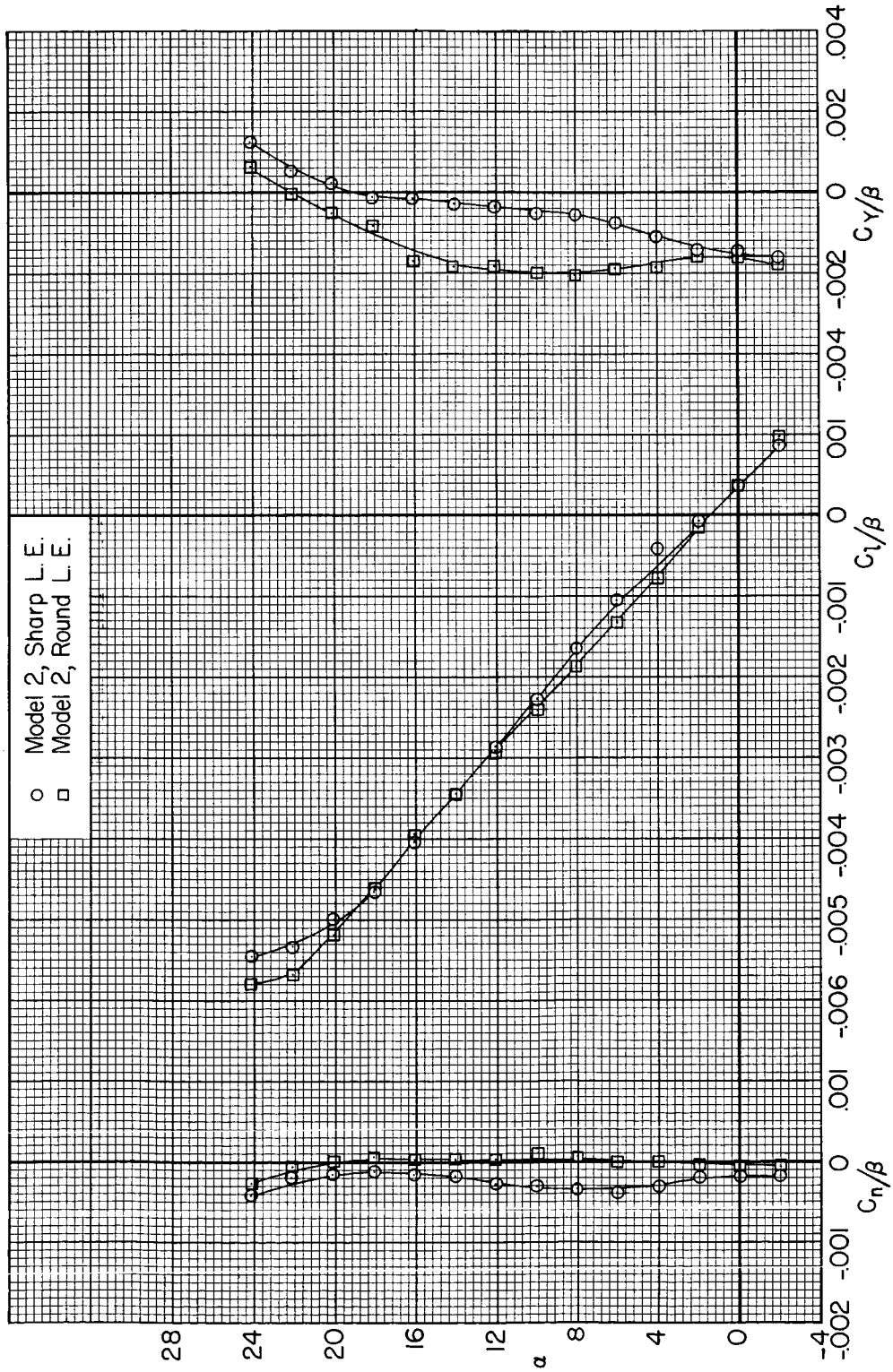

(b) α variable, β = ~9°

Figure 10.- Concluded.

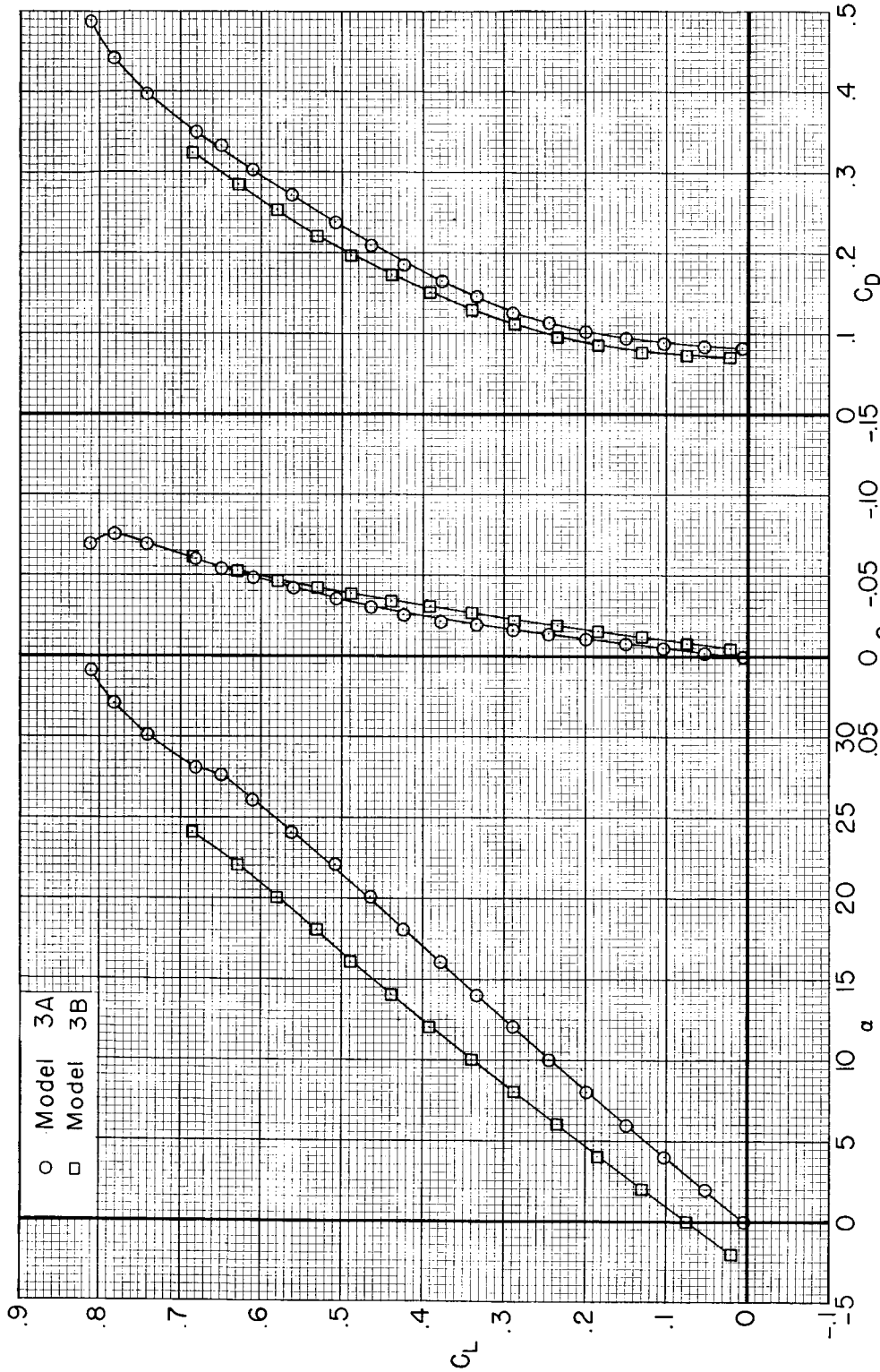

(a) Lift, drag, and pitching-moment characteristics.

Figure 11.- The longitudinal aerodynamic characteristics of models 3A and 3B; M = 0.25, R = 4.4 million, β = 0°.

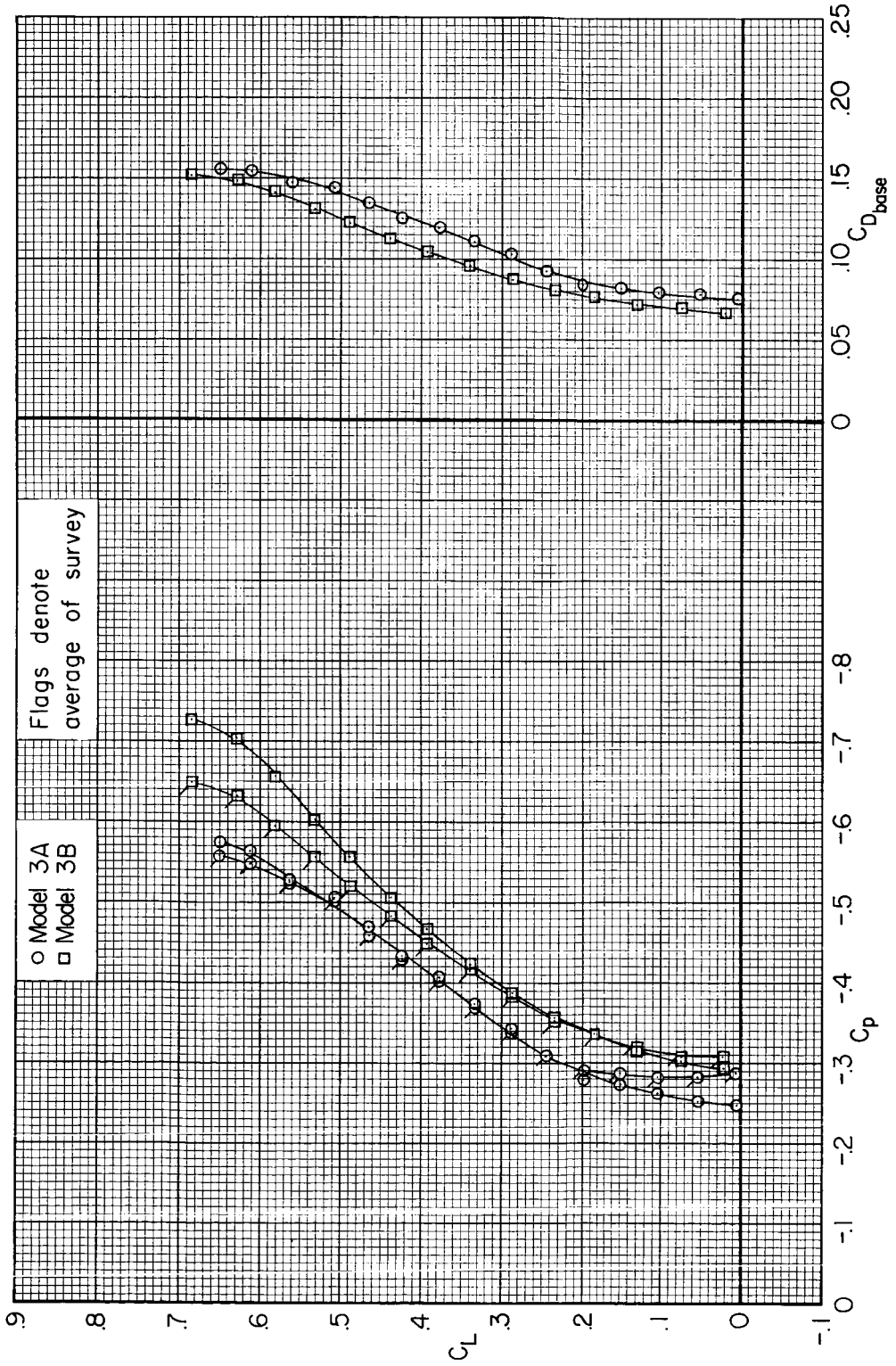

(b) Base pressure and base drag coefficients.

Figure 11.- Continued.

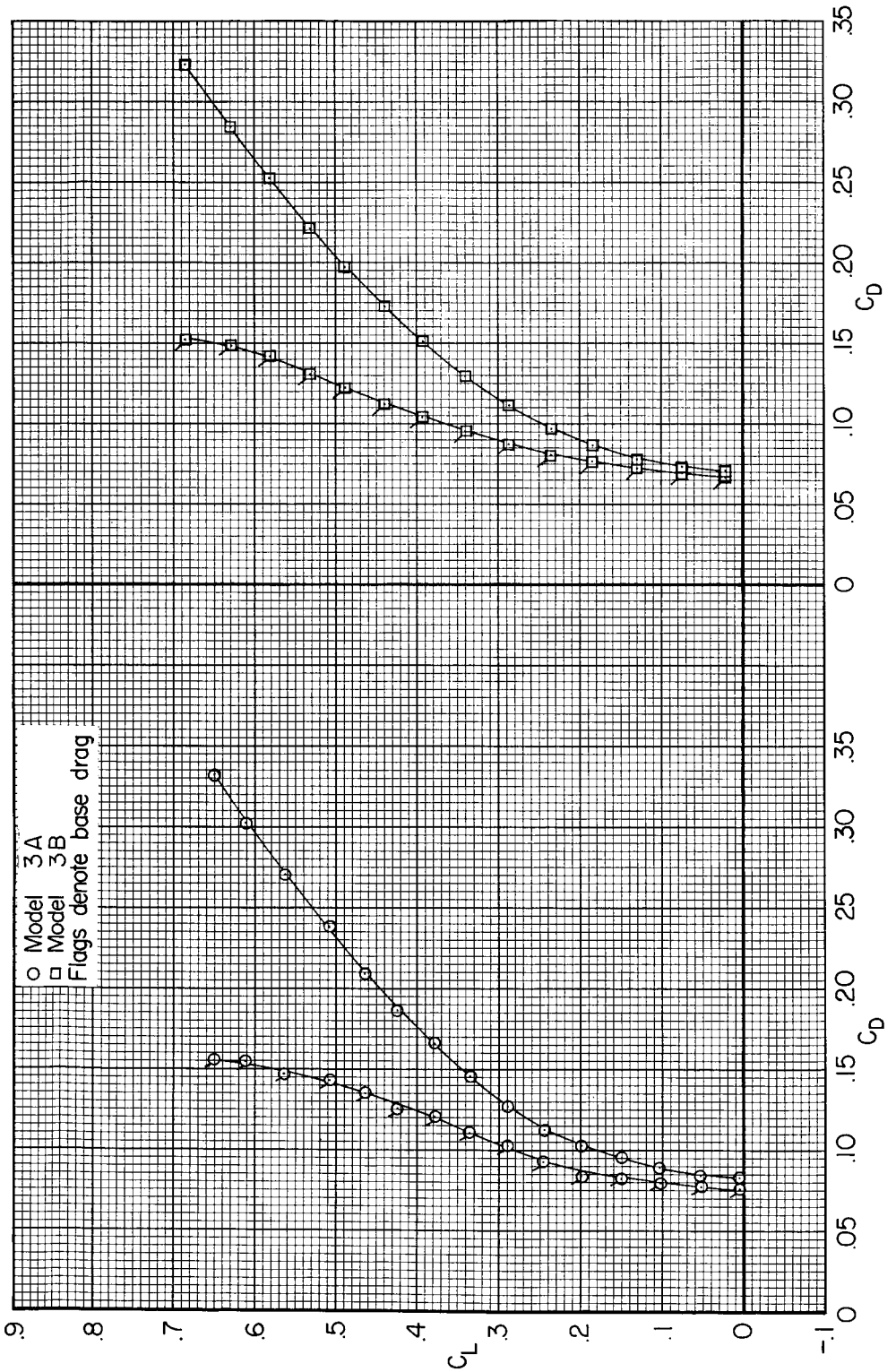

(c) Total drag and base drag coefficients.

Figure 11.- Concluded.

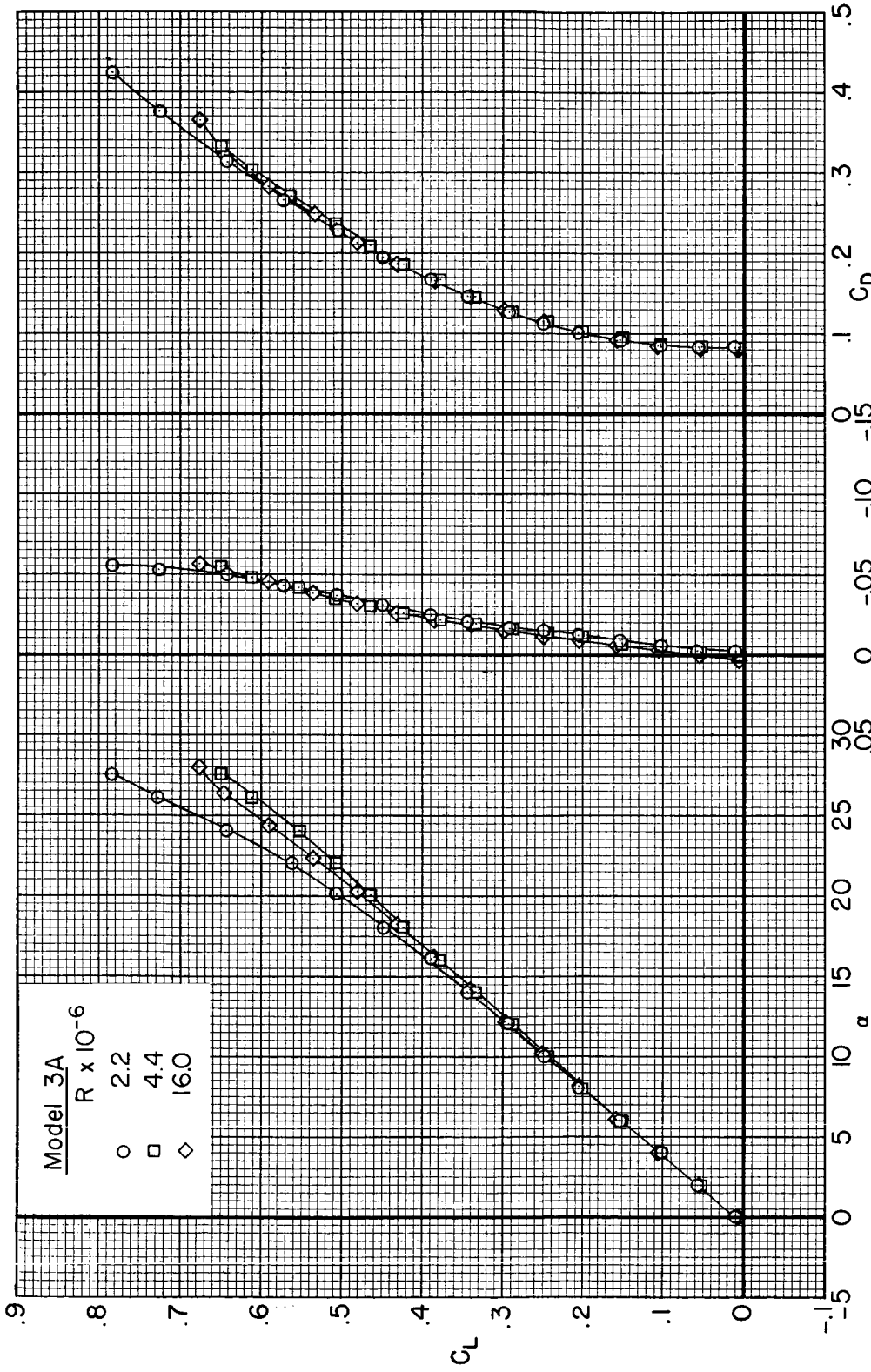

Figure 12.- The effects of Reynolds number on the longitudinal aerodynamic characteristics of model 3A; M = 0.25, $\beta = 0^{\circ}$.

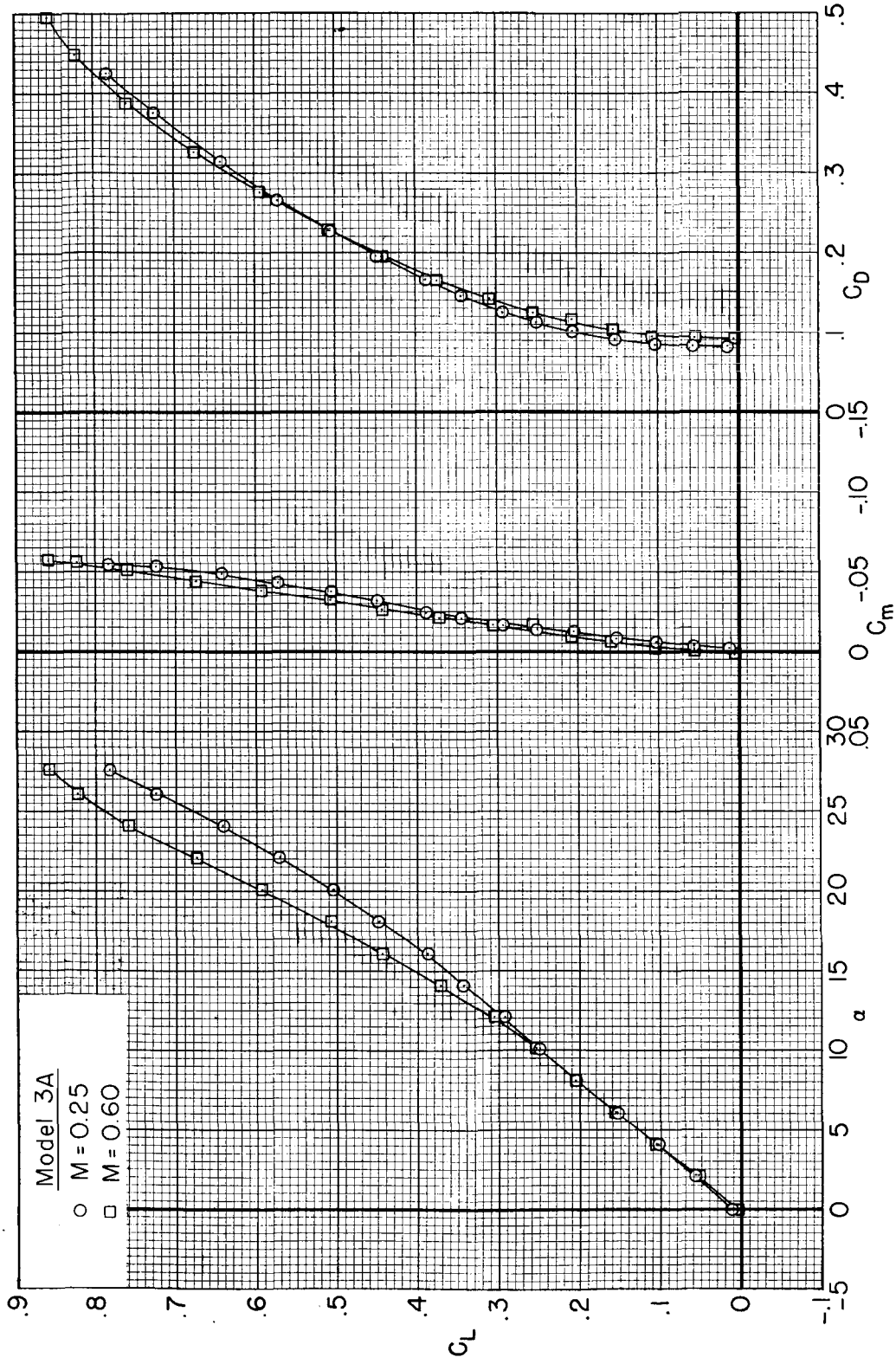

Figure 13.- The effects of Mach number on the longitudinal aerodynamic characteristics of model 3A; R = 2.2 million, β = 0°.

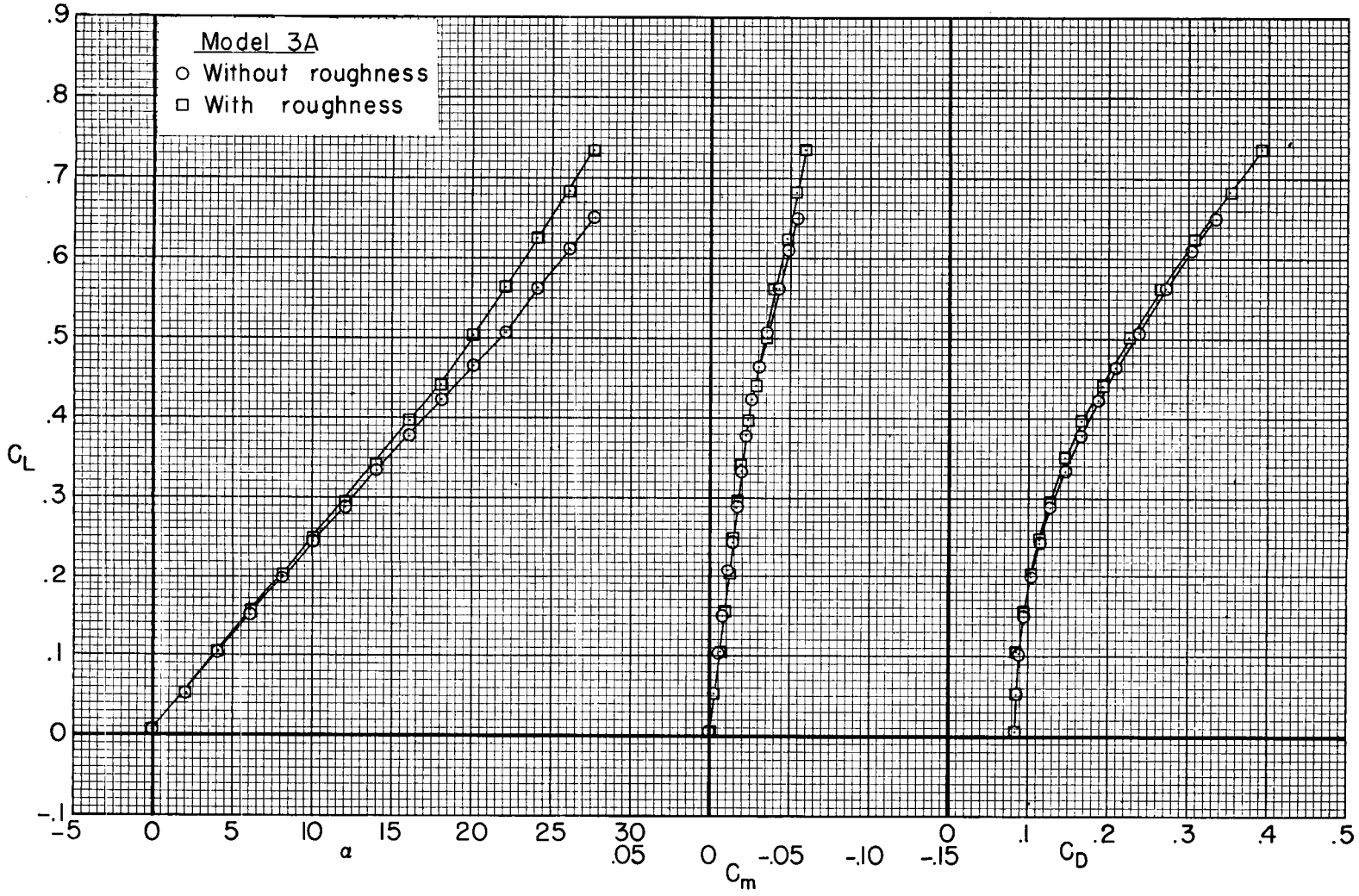

Figure 14.- The effects of leading-edge roughness on the longitudinal aerodynamic characteristics of model 3A; M = 0.25, R = 4.4 million, $\beta = 0^{\circ}$.

CONFIDENTIAL

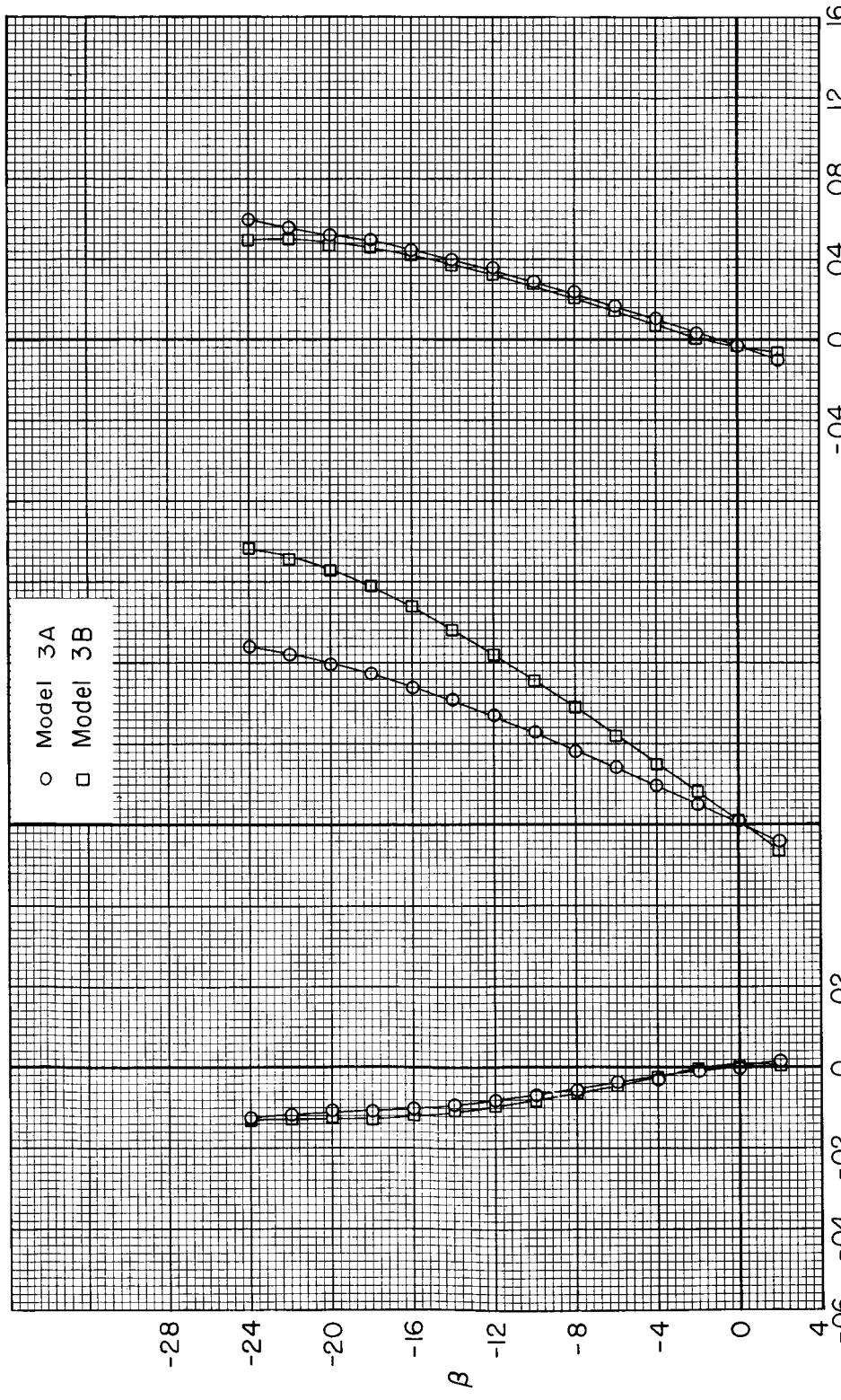

(a) β variable, α = ~9°

Figure 15.- The lateral and directional characteristics of models 3A and 3B; M = 0.25, R = 4.4 million.

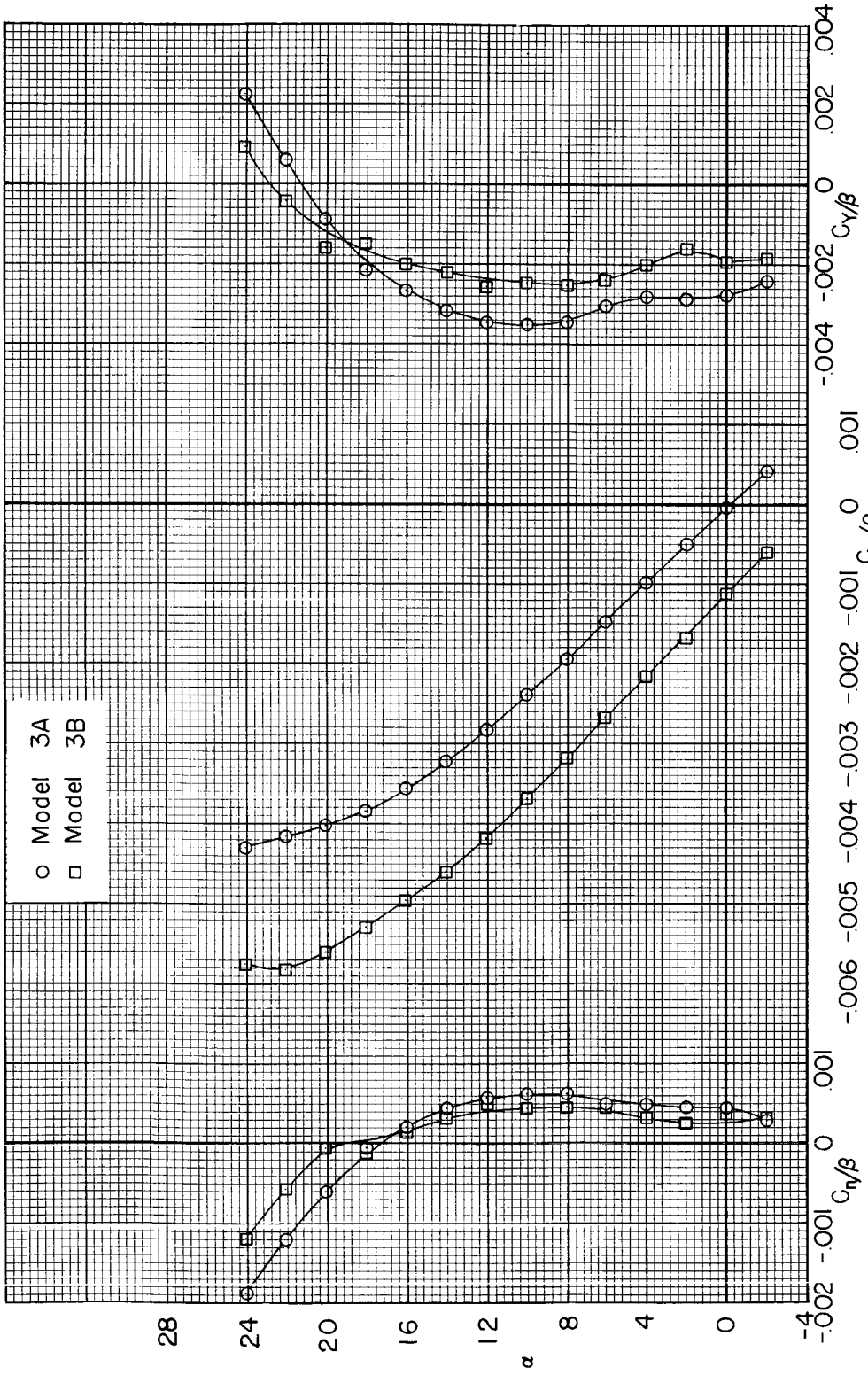

(b) α variable, β = ~9°

Figure 15.- Concluded.

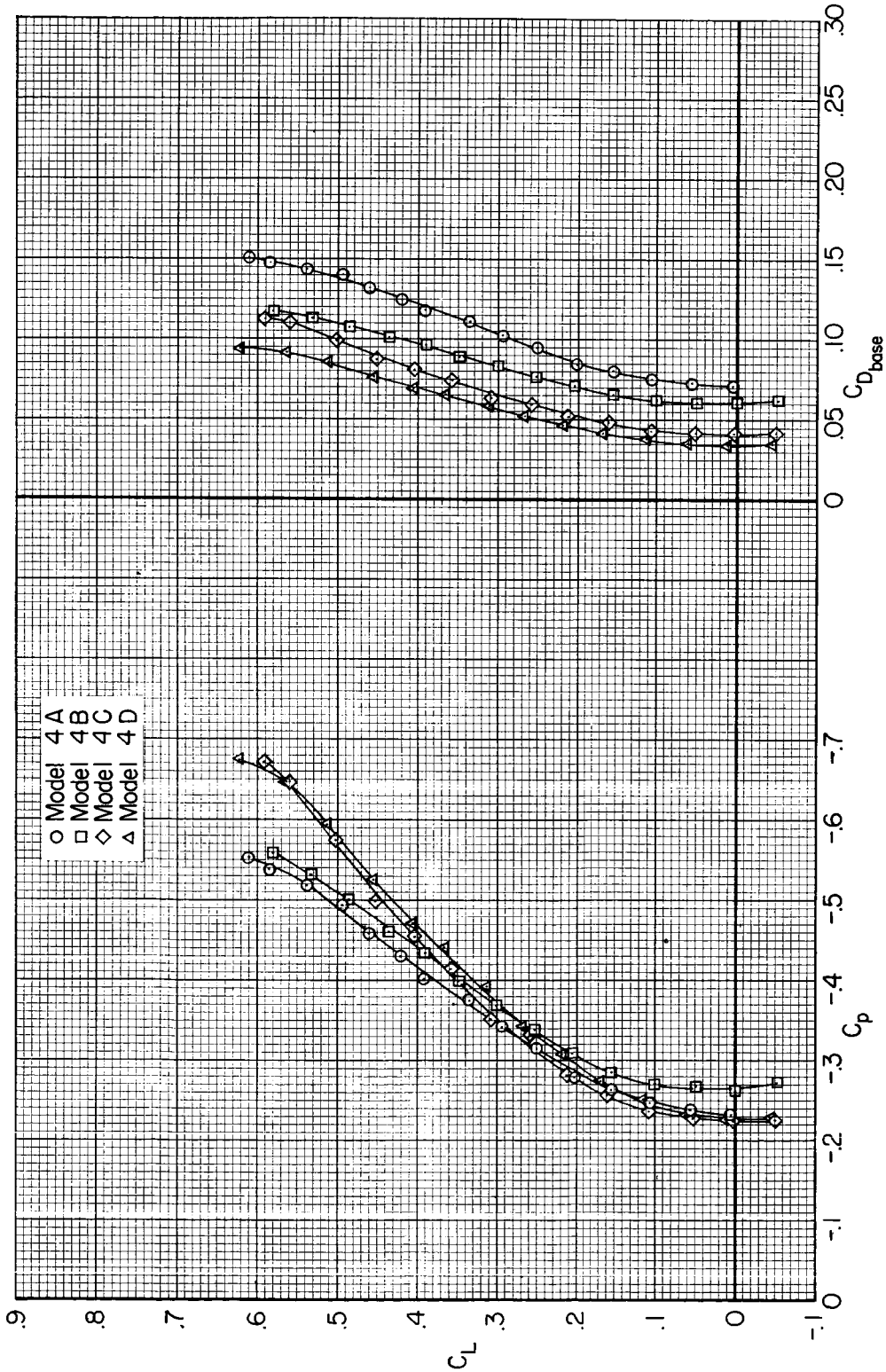

(b) Base pressure and base drag coefficients.

Figure 16.- Continued.

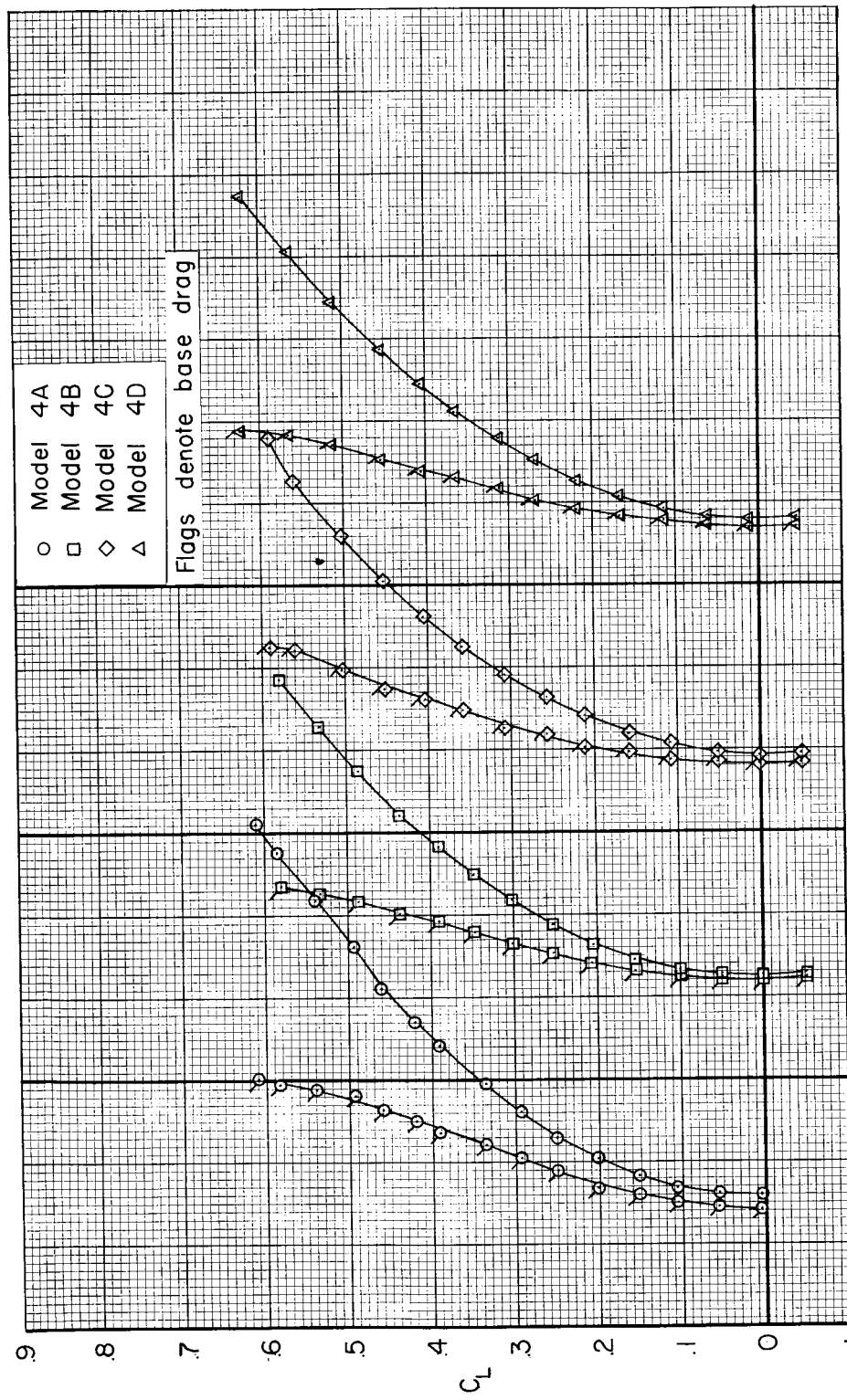

(c) Total drag and base drag coefficients.

Figure 16.- Concluded.

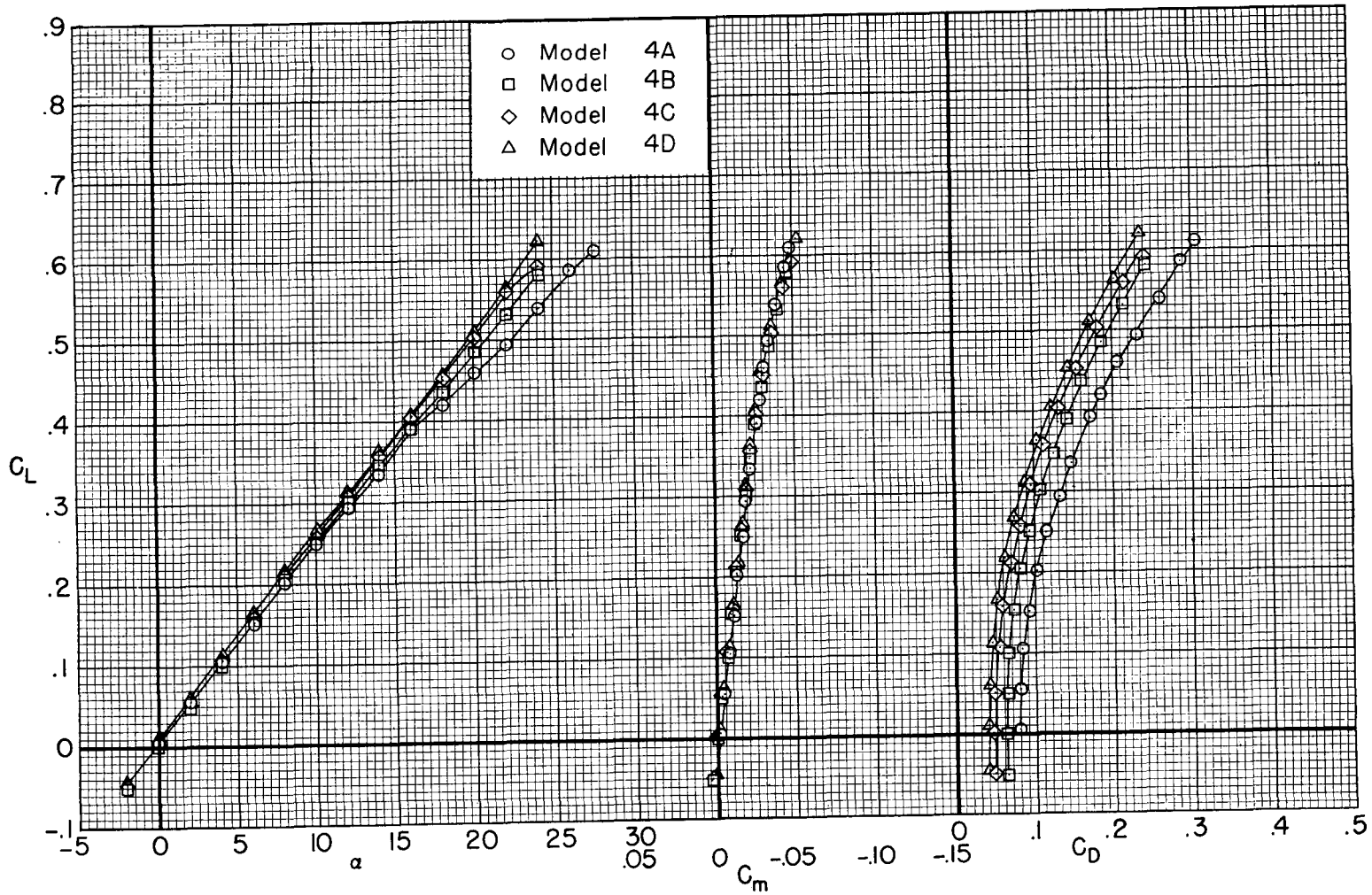

(a) Lift, drag, and pitching-moment characteristics.

Figure 16.- The longitudinal aerodynamic characteristics of models 4A, 4B, 4C, and 4D; M = 0.25, R = 4.4 million, $\beta = 0^\circ$.

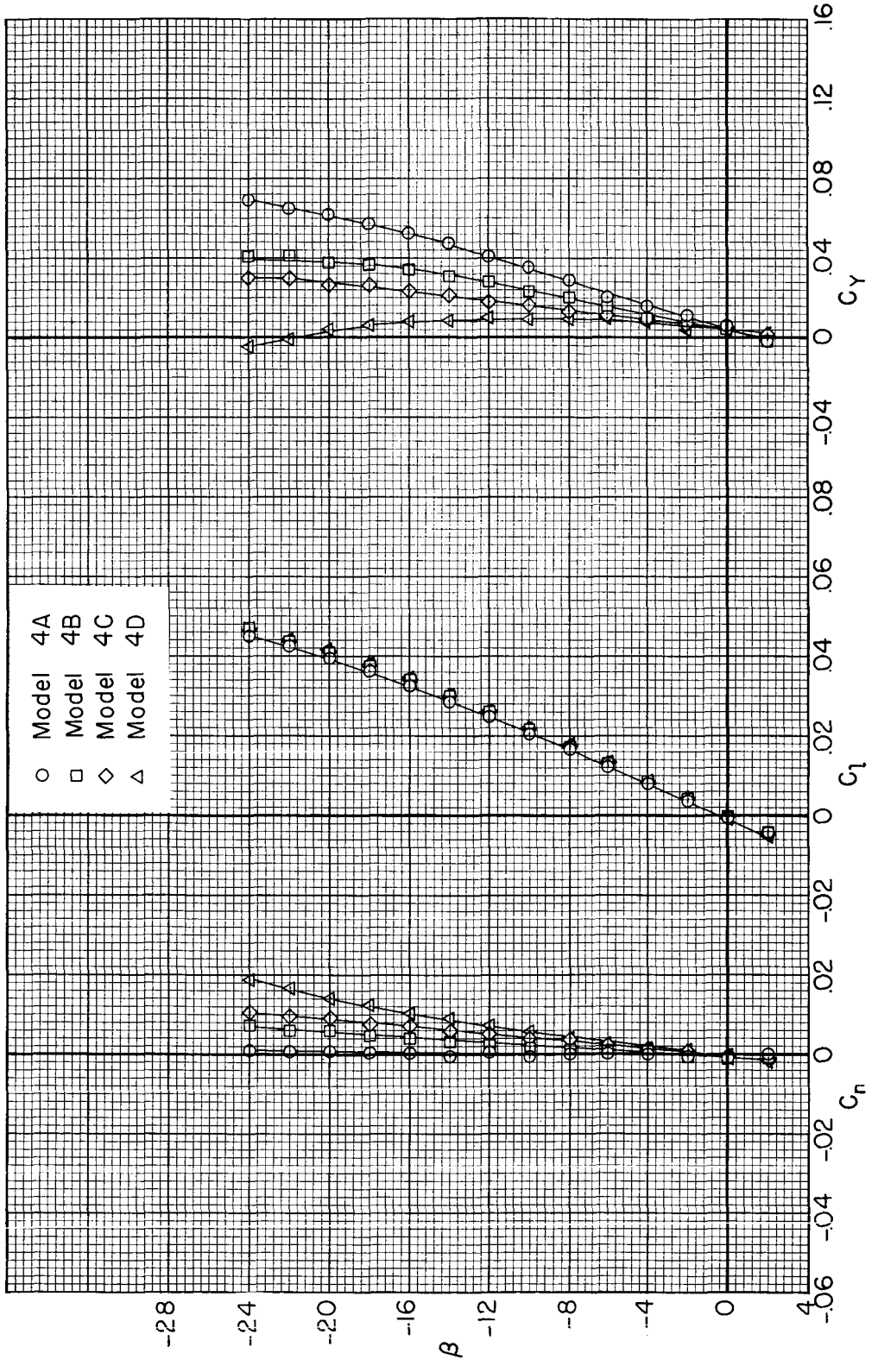

(a) β variable, α = ~9°

Figure 17.- The lateral and directional characteristics of models 4A, 4B, 4C, and 4D; M = 0.25, R = 4.4 million.

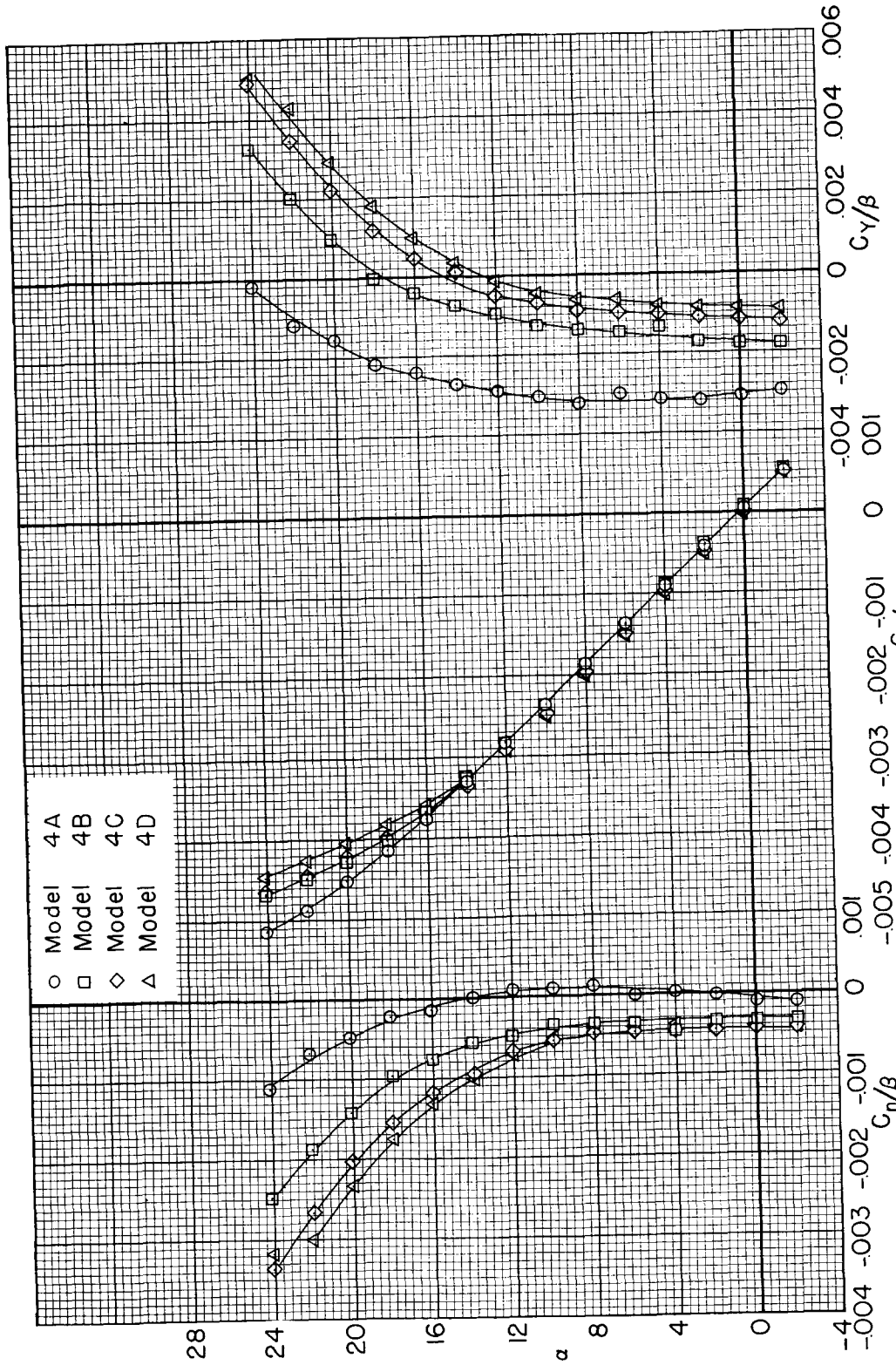

(b) α variable, β = ~9°.

Figure 17.- Concluded.

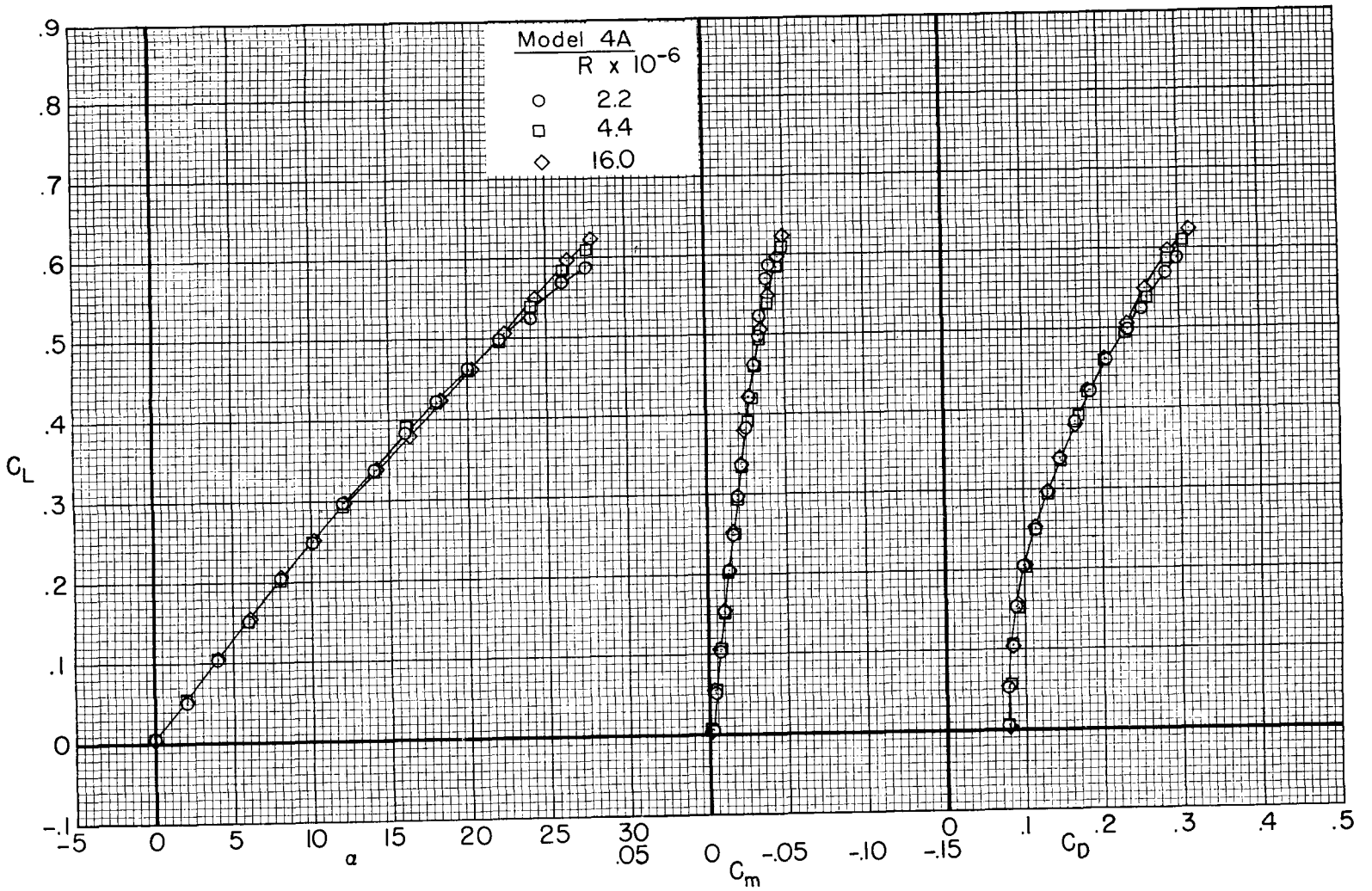

Figure 19.- The effects of Reynolds number on the longitudinal aerodynamic characteristics of model 4A; M = 0.25, $\beta = 0^{\circ}$.

CONFIDENTIAL

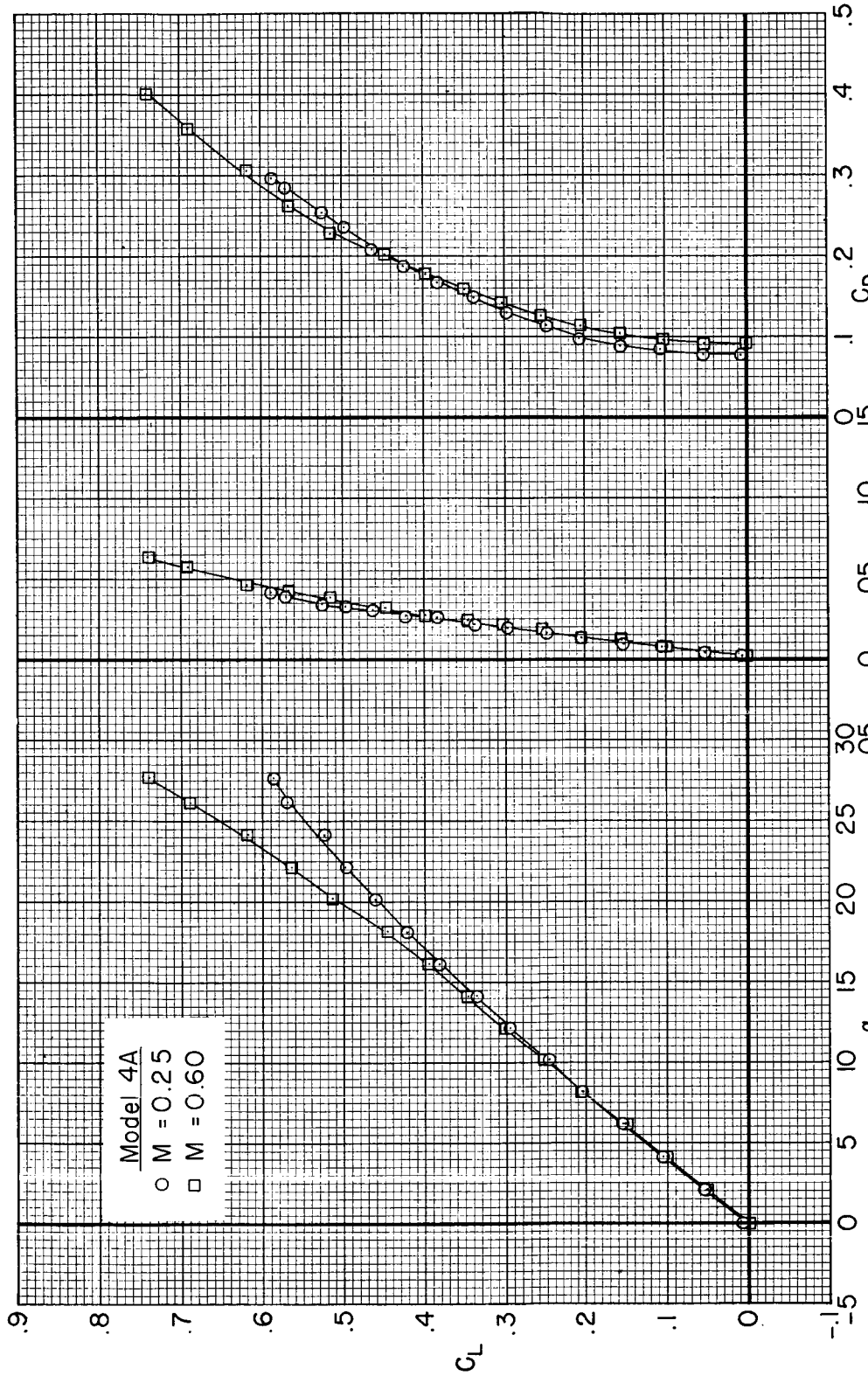

Figure 20.- The effects of Mach number on the longitudinal aerodynamic characteristics of model 4A; R = 2.2 million, $\beta = 0^{\circ}$.

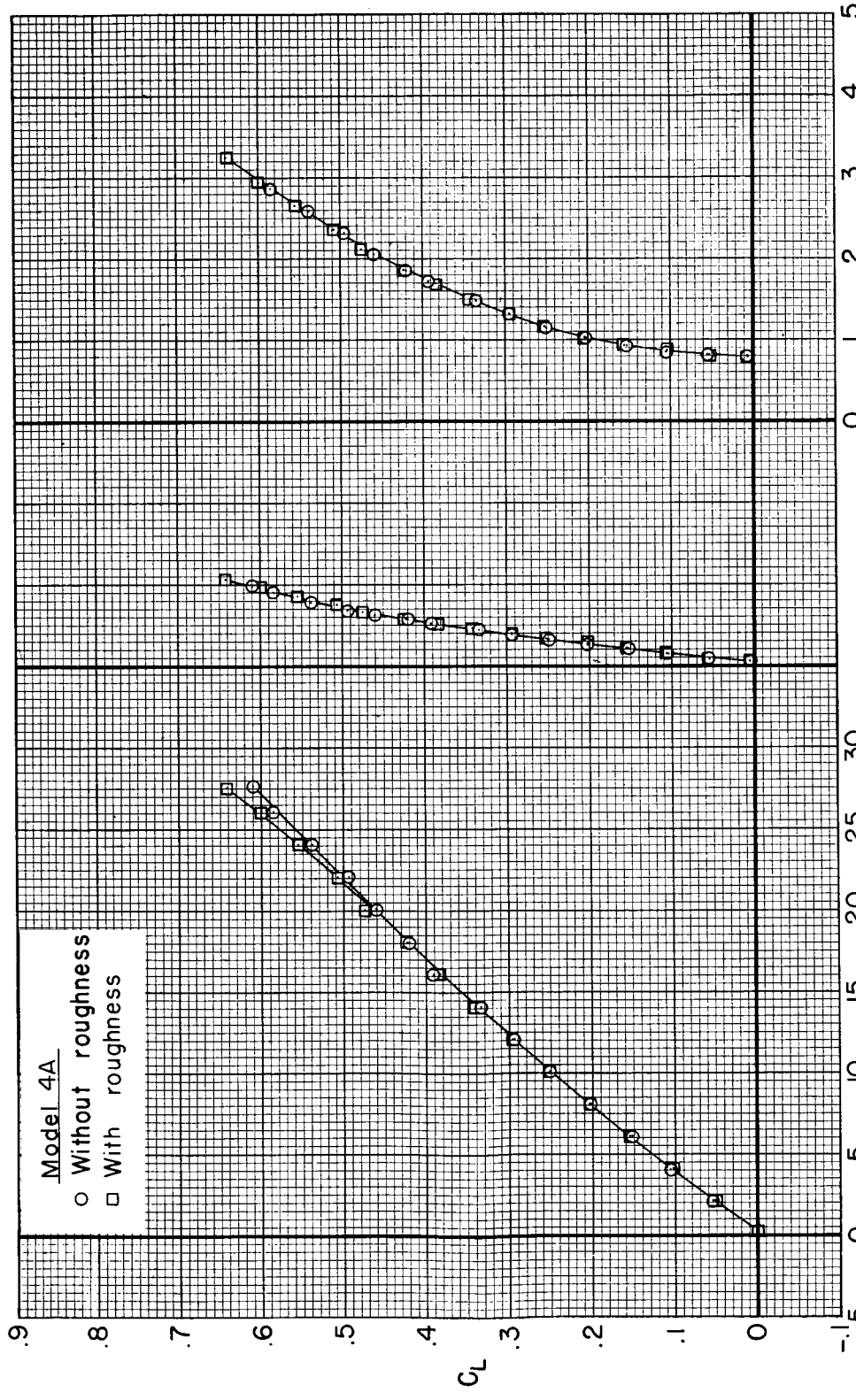

Figure 21.- The effects of leading-edge roughness on the longitudinal aerodynamic characteristics of model 4A; M = 0.25, R = 4.4 million, $\beta = 0^{\circ}$.

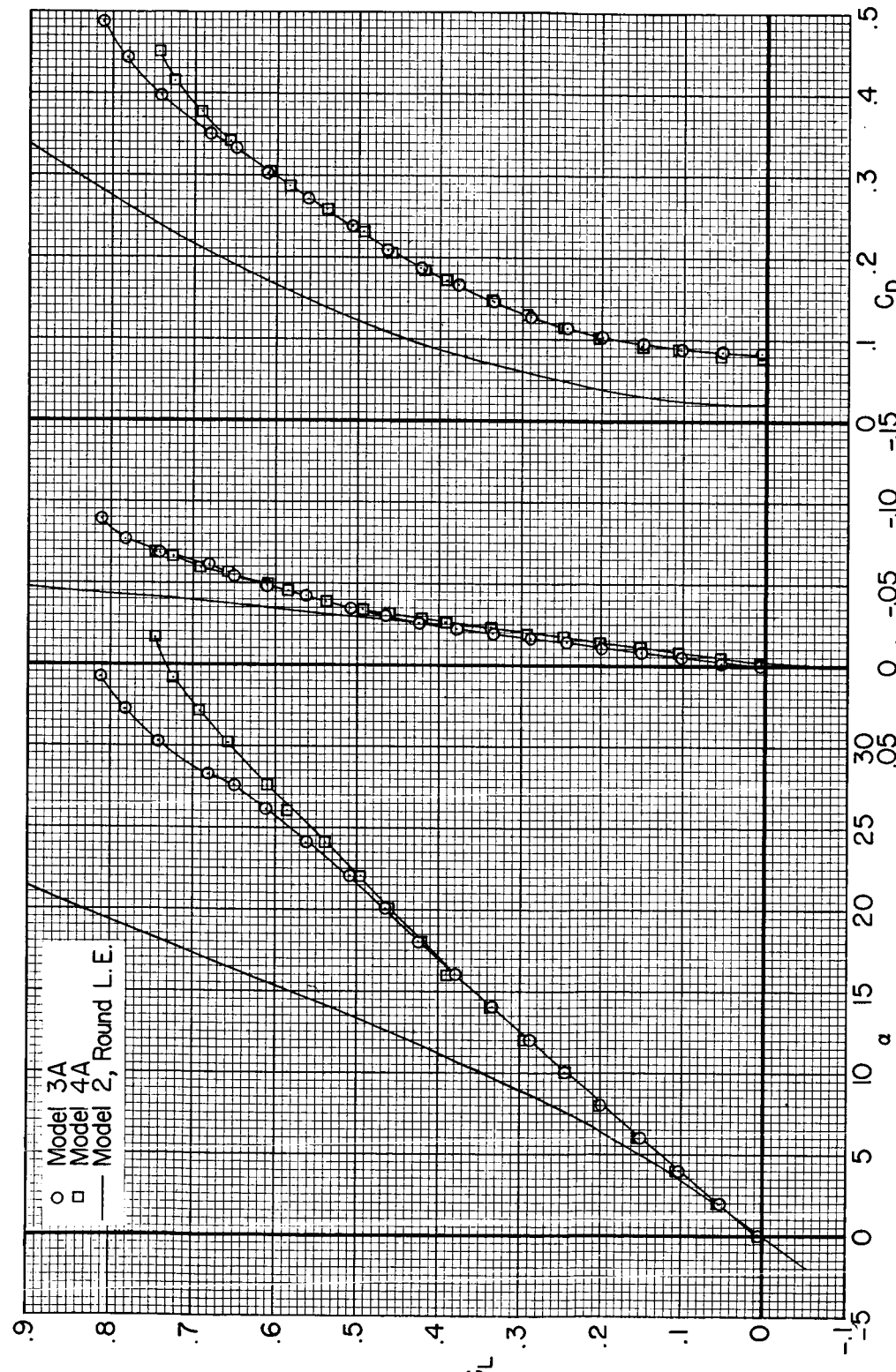

Figure 18.- Comparison of the longitudinal aerodynamic characteristics of models 3A and 4A with those of flat-plate model 2 with round leading edges; M = 0.25, R = 4.4 million, β = 0°.

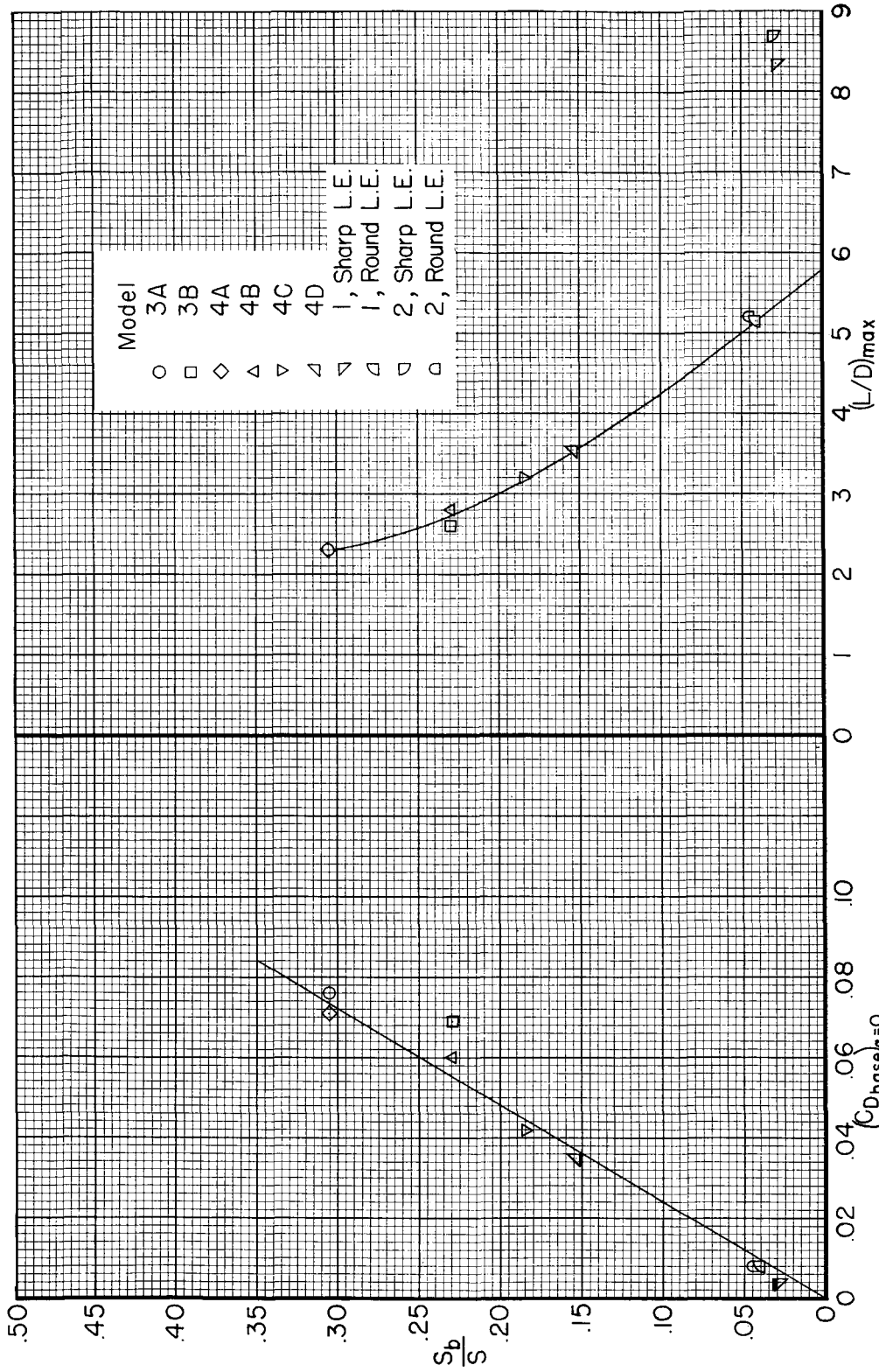

Figure 23.- Base drag coefficient and maximum lift-drag ratios as functions of ratio of base area to plan-form area; M = 0.25, R = 4.4 million, $\beta = 0^{\circ}$.

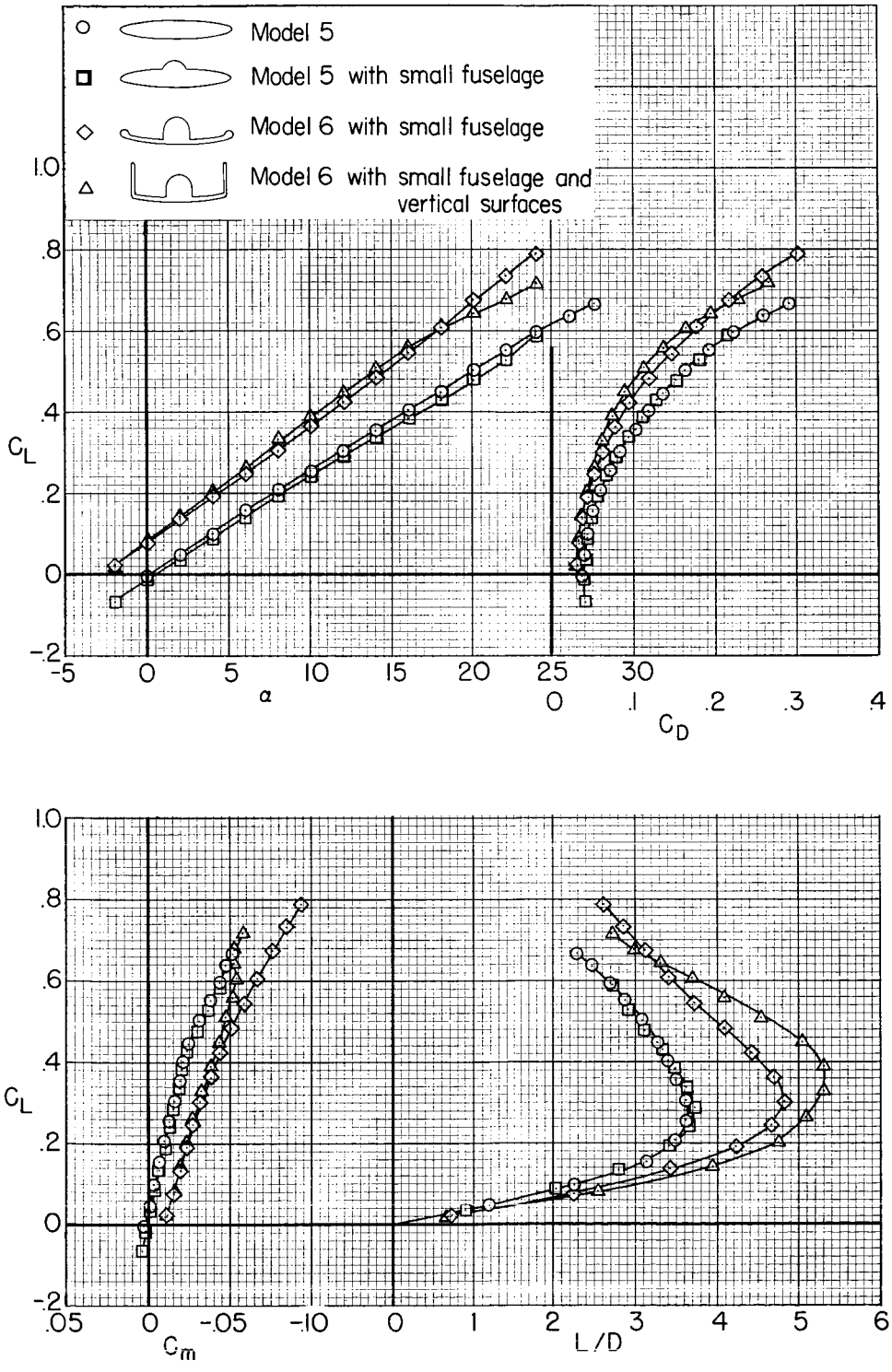

Figure 24.- The effects of configuration changes on the longitudinal aerodynamic characteristics of models utilizing the small fuselage; M = 0.25, R = 4.4 million, $\beta = 0^\circ$.

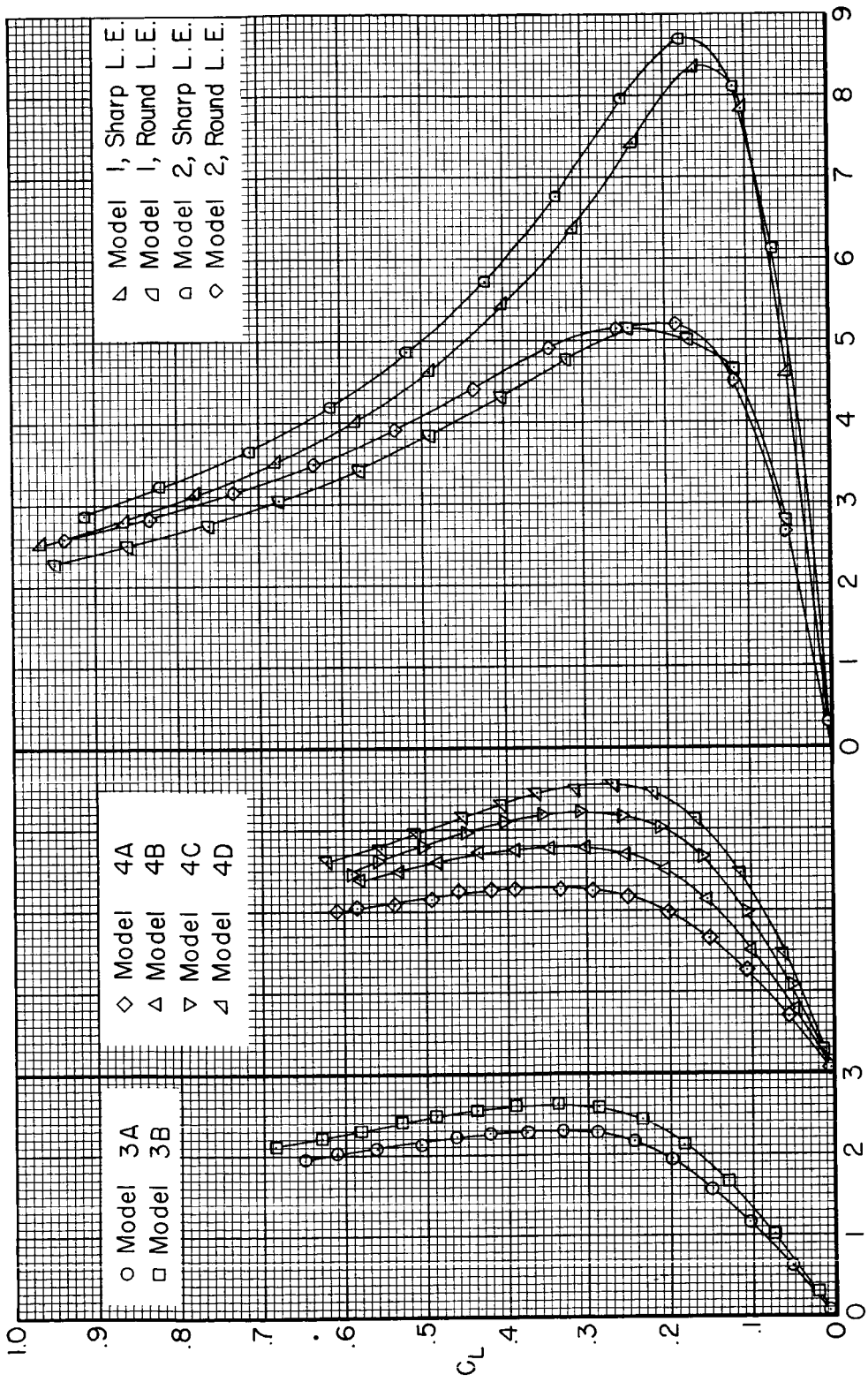

Figure 22.- Lift-drag ratios of the models as a function of lift coefficient; M = 0.25, R = 4.4 million, $\beta = 0^{\circ}$.

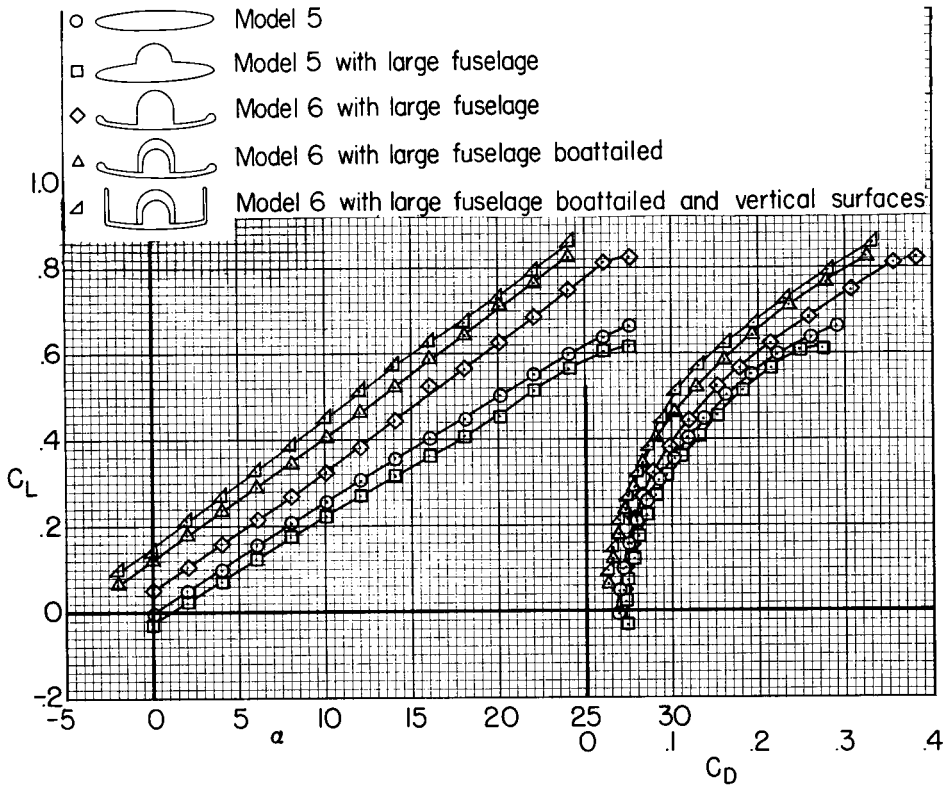

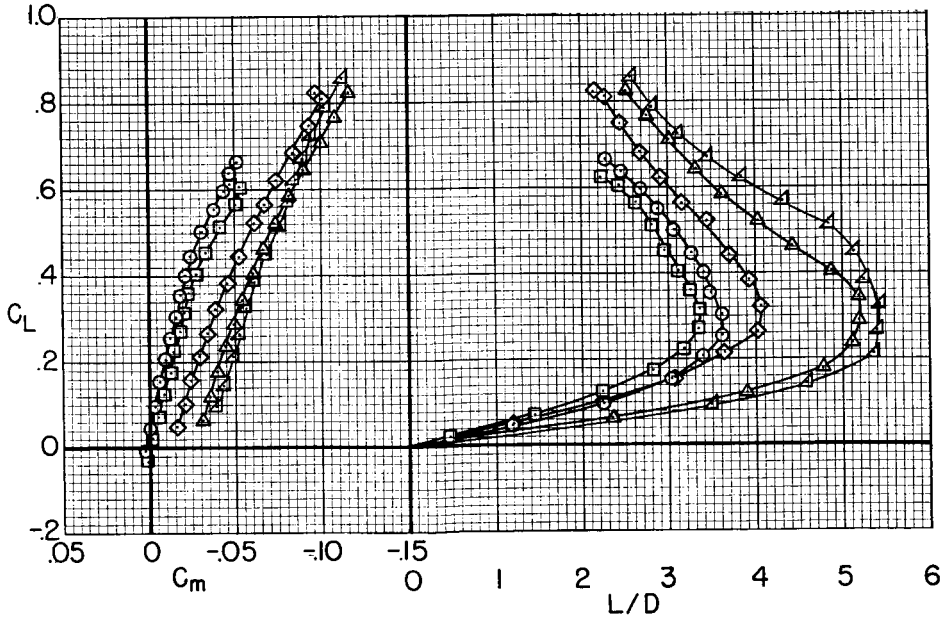

Figure 25.- The effects of configuration changes on the longitudinal aerodynamic characteristics of models utilizing the large fuselage; M = 0.25, R = 4.4 million, $\beta = 0^{\circ}$.

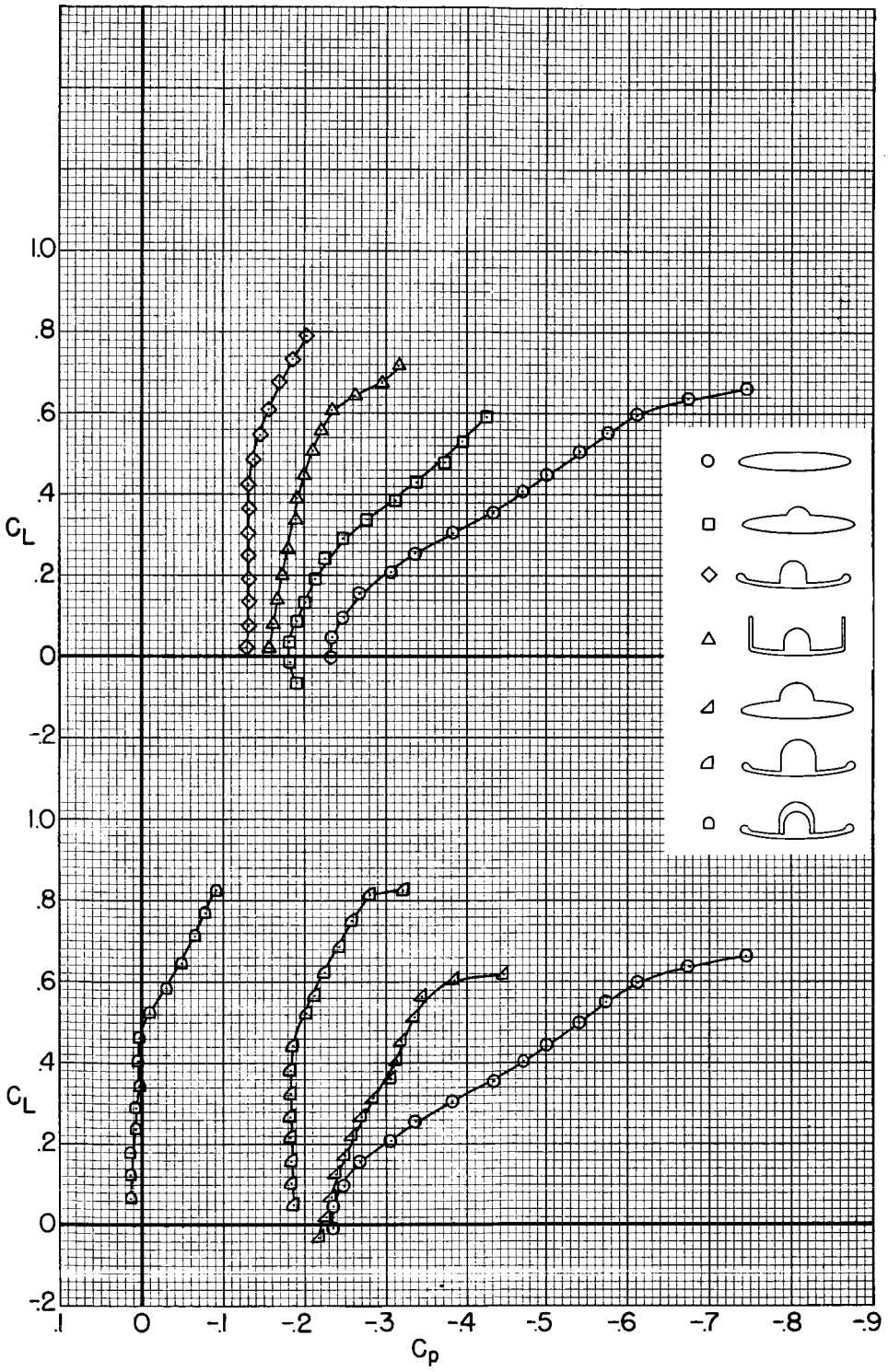

Figure 26.- Base-pressure coefficients of several configurations; M = 0.25, R = 4.4 million, $\beta = 0^{\circ}$.

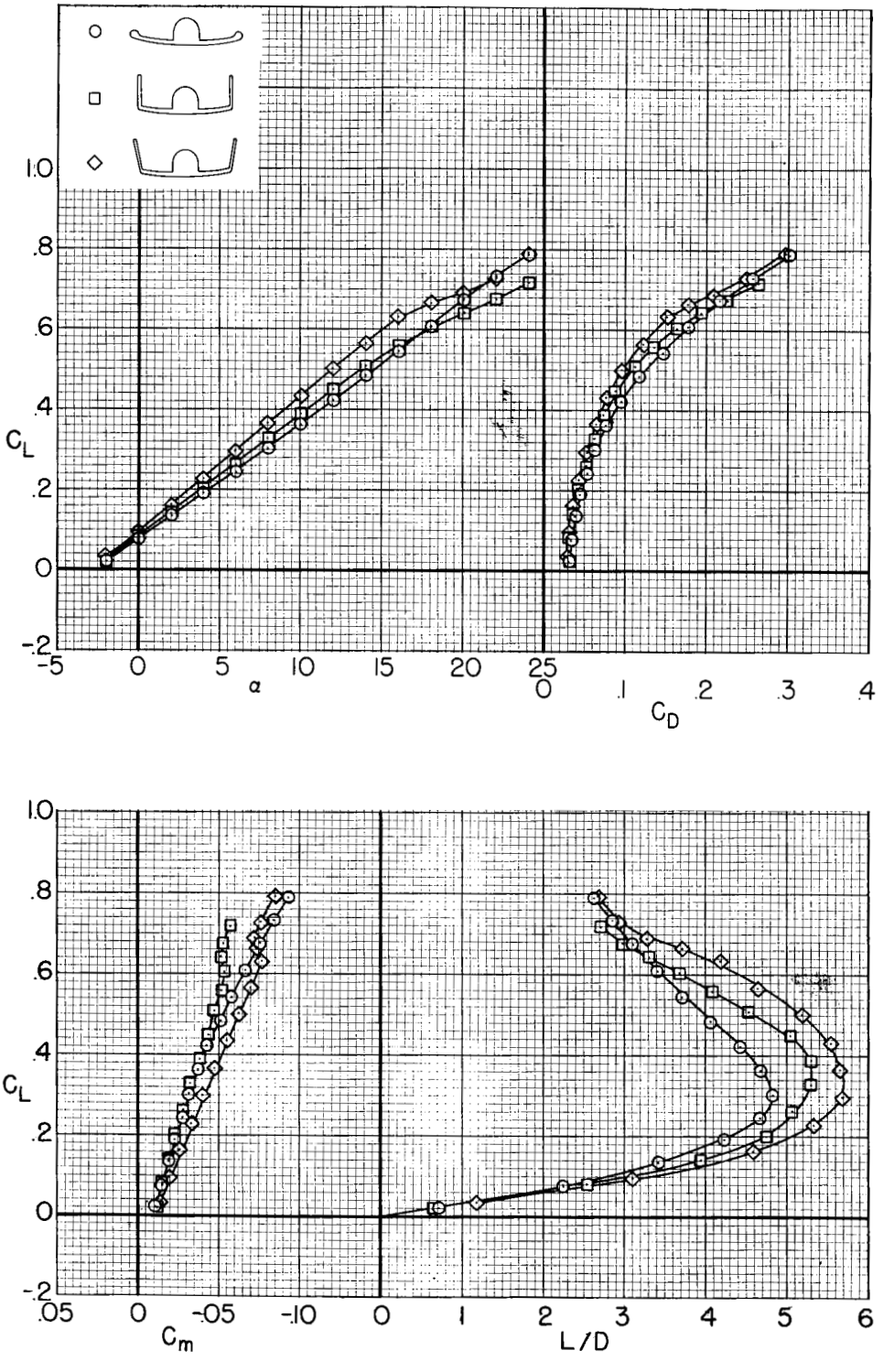

Figure 27.- The effects of vertical surfaces and vertical surface angle on the longitudinal aerodynamic characteristics of model 6 with the small fuselage; M = 0.25, R = 4.4 million, $\beta = 0^{\circ}$.

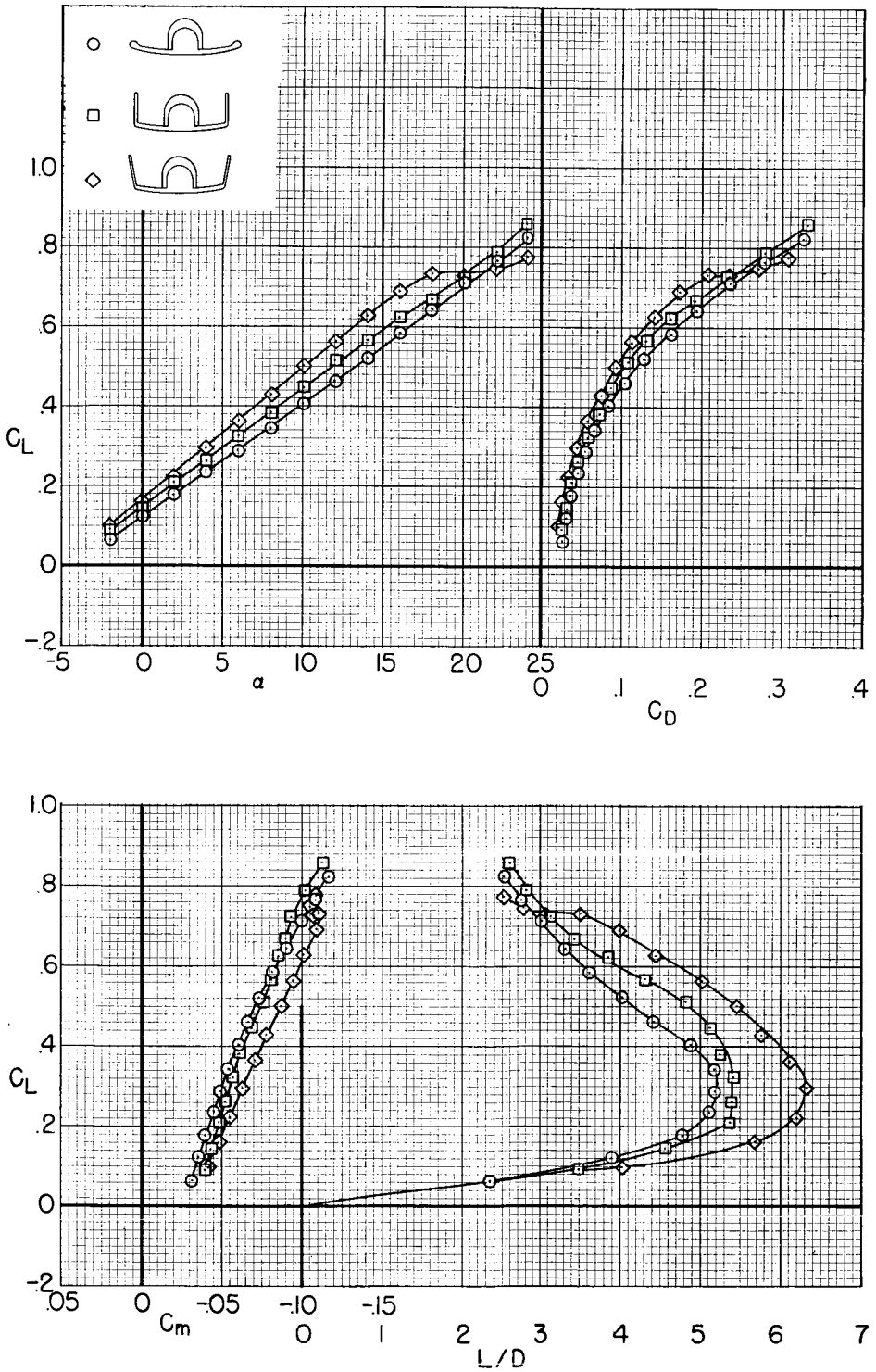

Figure 28.- The effects of vertical surfaces and vertical surface angle on the longitudinal aerodynamic characteristics of model 6 with the large, boattailed fuselage; M = 0.25, R = 4.4 million, $\beta = 0^{\circ}$.

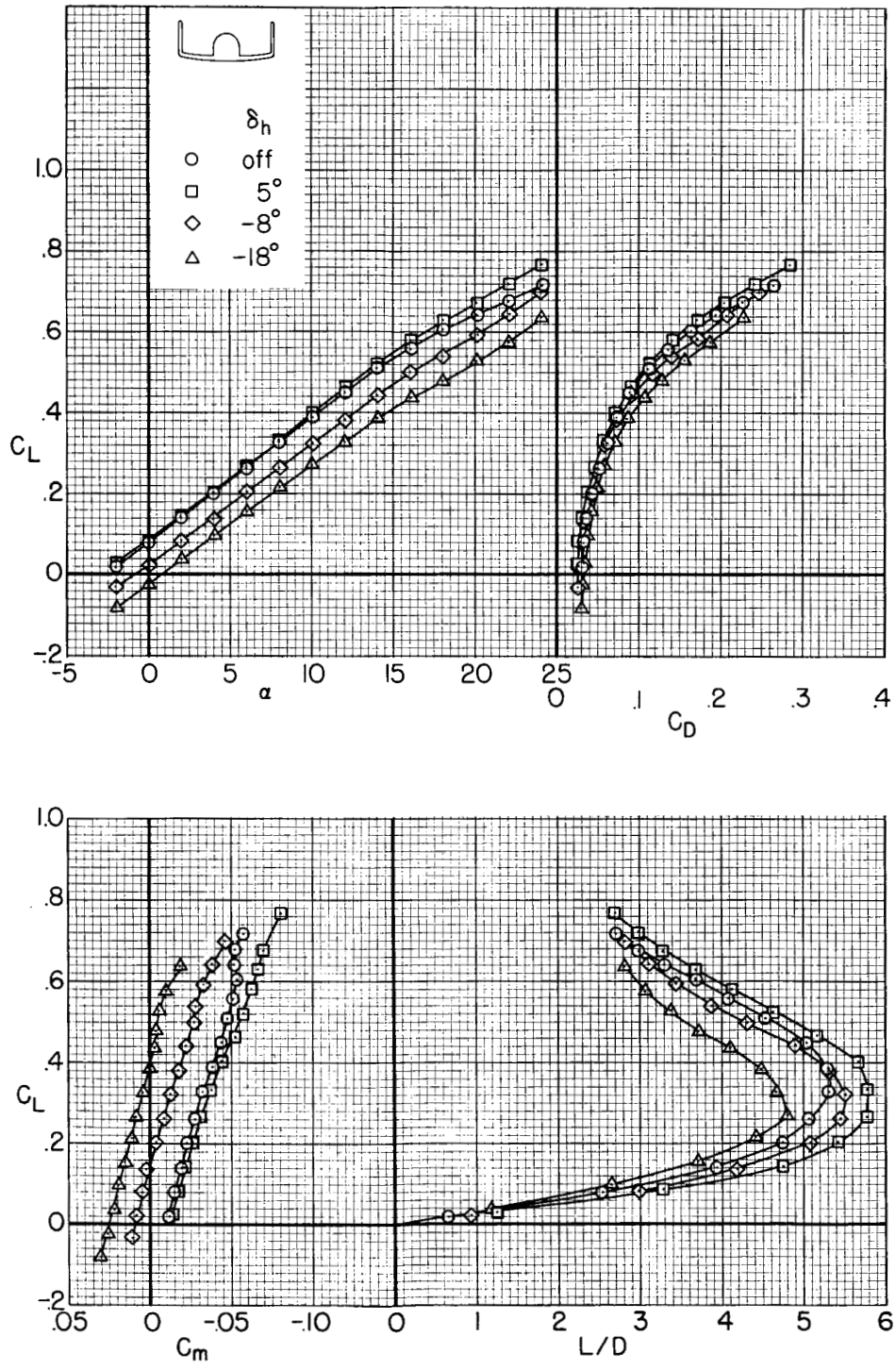

Figure 29.- The effects of elevon control deflection on the longitudinal aerodynamic characteristics of model 6 with small fuselage and vertical surfaces (δ_r = 90°); M = 0.25, R = 4.4 million, β = 0°.

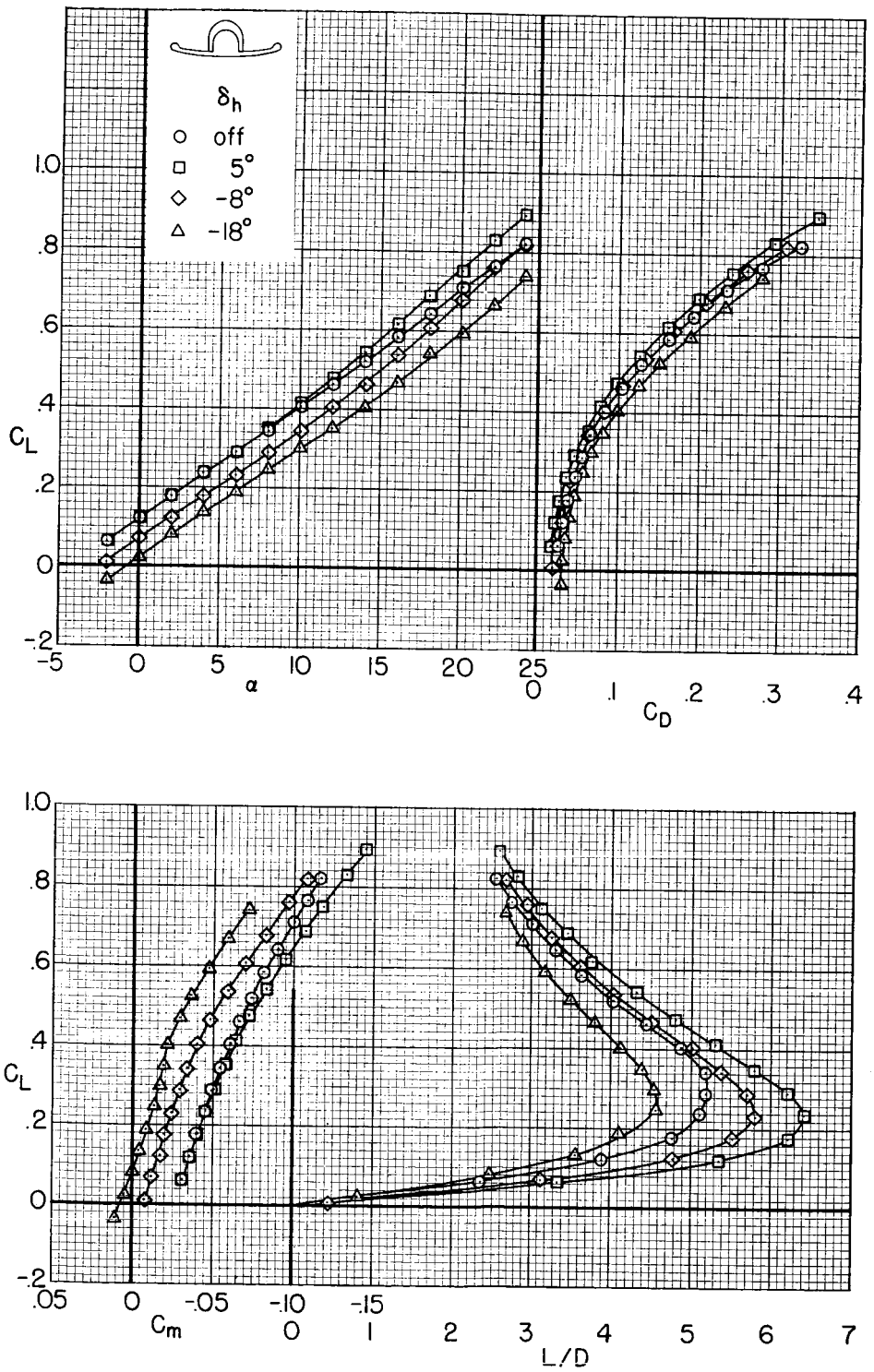

Figure 30.- The effects of elevon control deflection on the longitudinal aerodynamic characteristics of model 6 with large, boattailed fuselage; M = 0.25, R = 4.4 million, β = 0°.

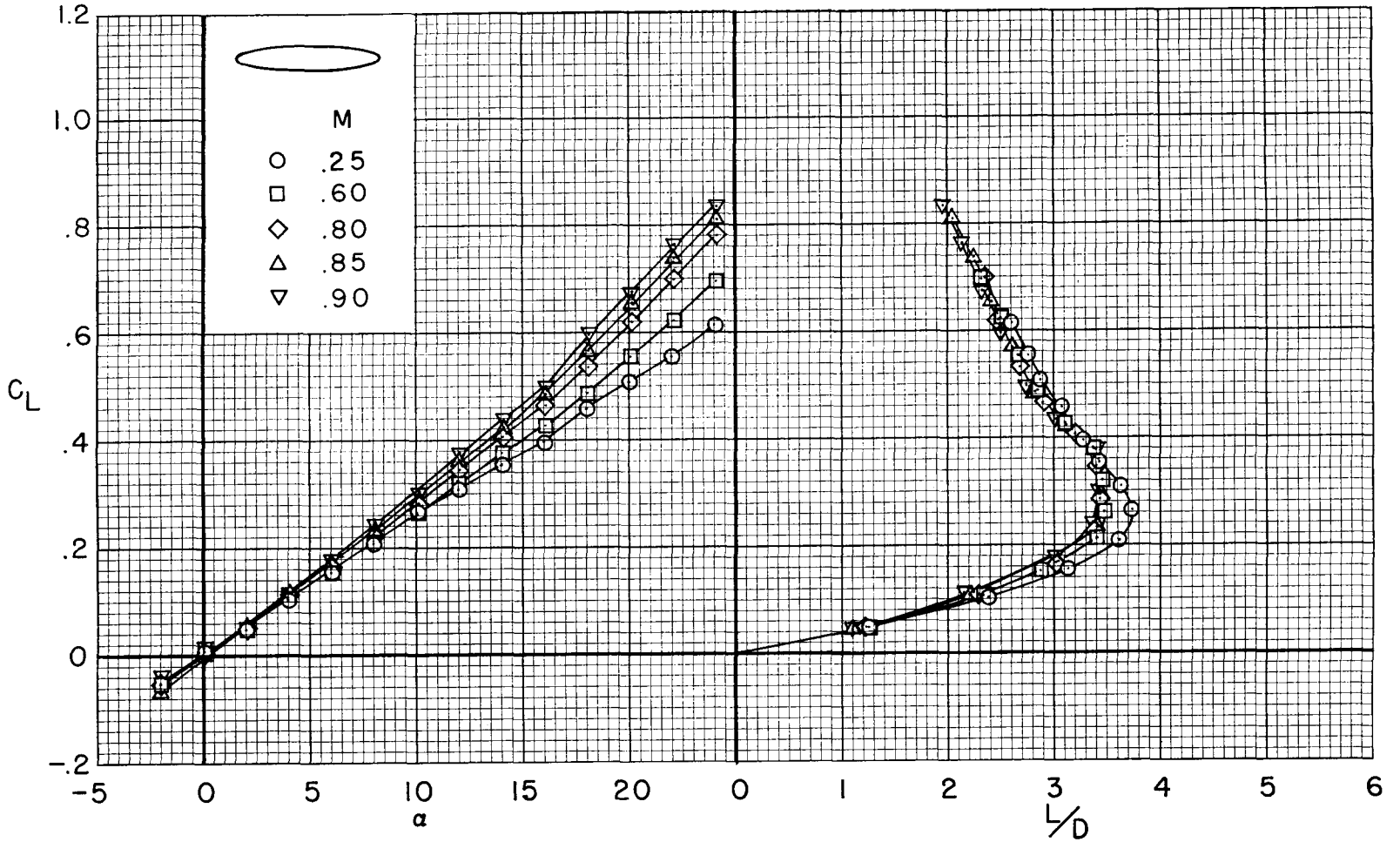

(a) Lift and L/D characteristics.

Figure 31.- The effects of Mach number on the longitudinal aerodynamic characteristics of model 5; R = 2.2 million, $\beta = 0^{o}$.

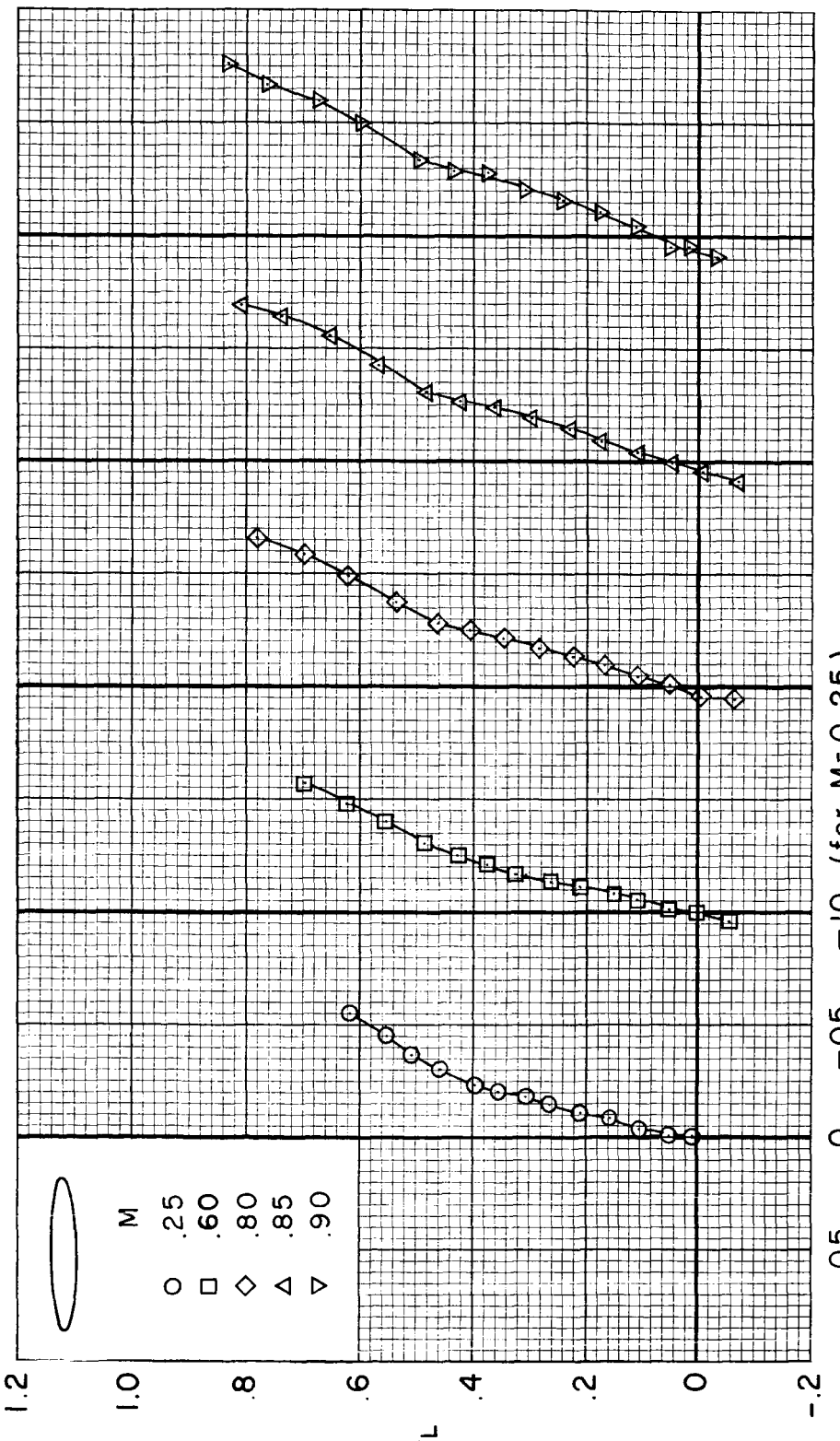

(b) Pitching-moment characteristics.

Figure 31.- Concluded.

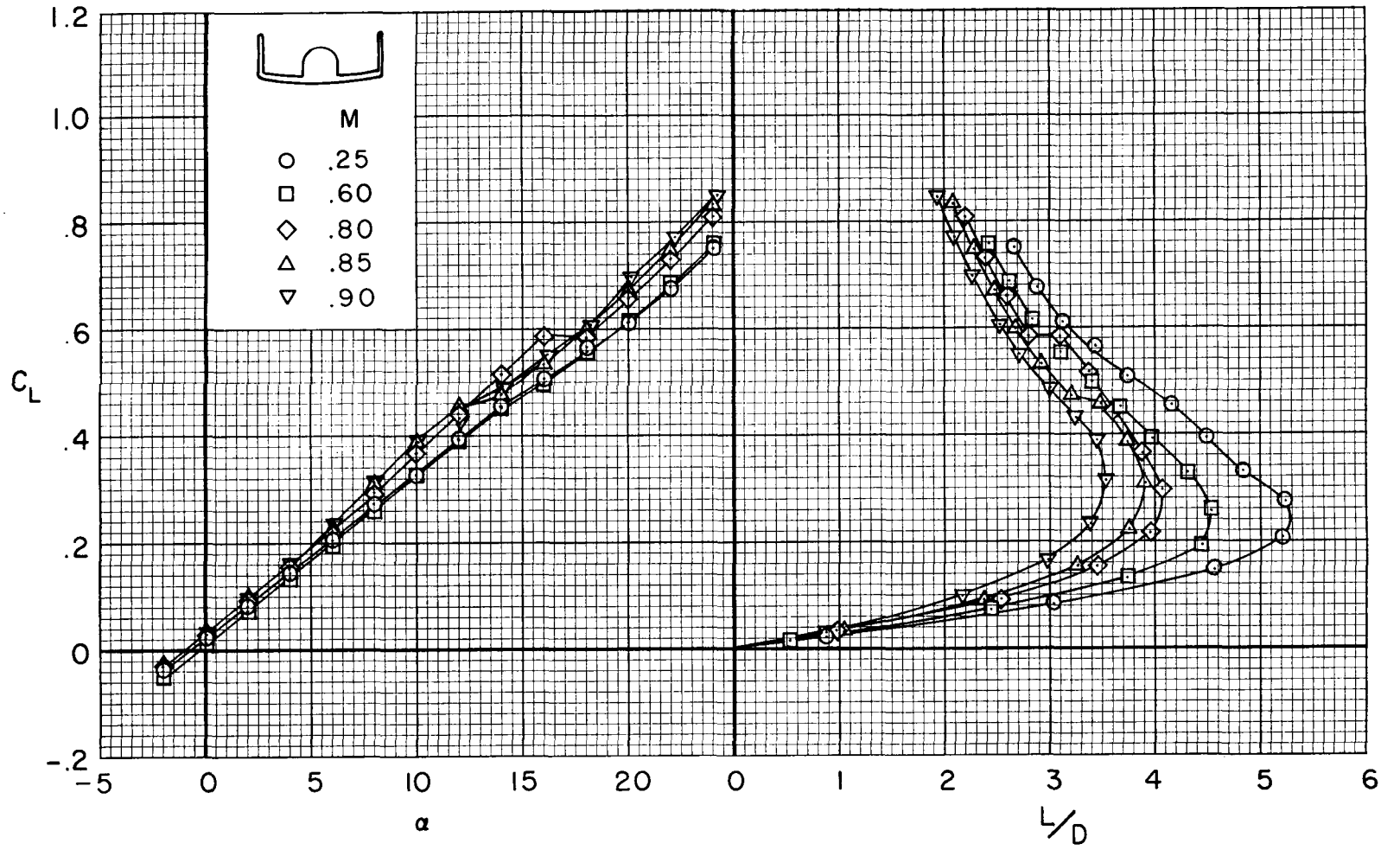

(a) Lift and L/D characteristics.

Figure 32.- The effects of Mach number on the longitudinal aerodynamic characteristics of model 6 with small fuselage, vertical surfaces ($\delta_r = 90^\circ$), and elevon controls ($\delta_e = -8^\circ$); R = 2.2 million, $\beta = 0^\circ$.

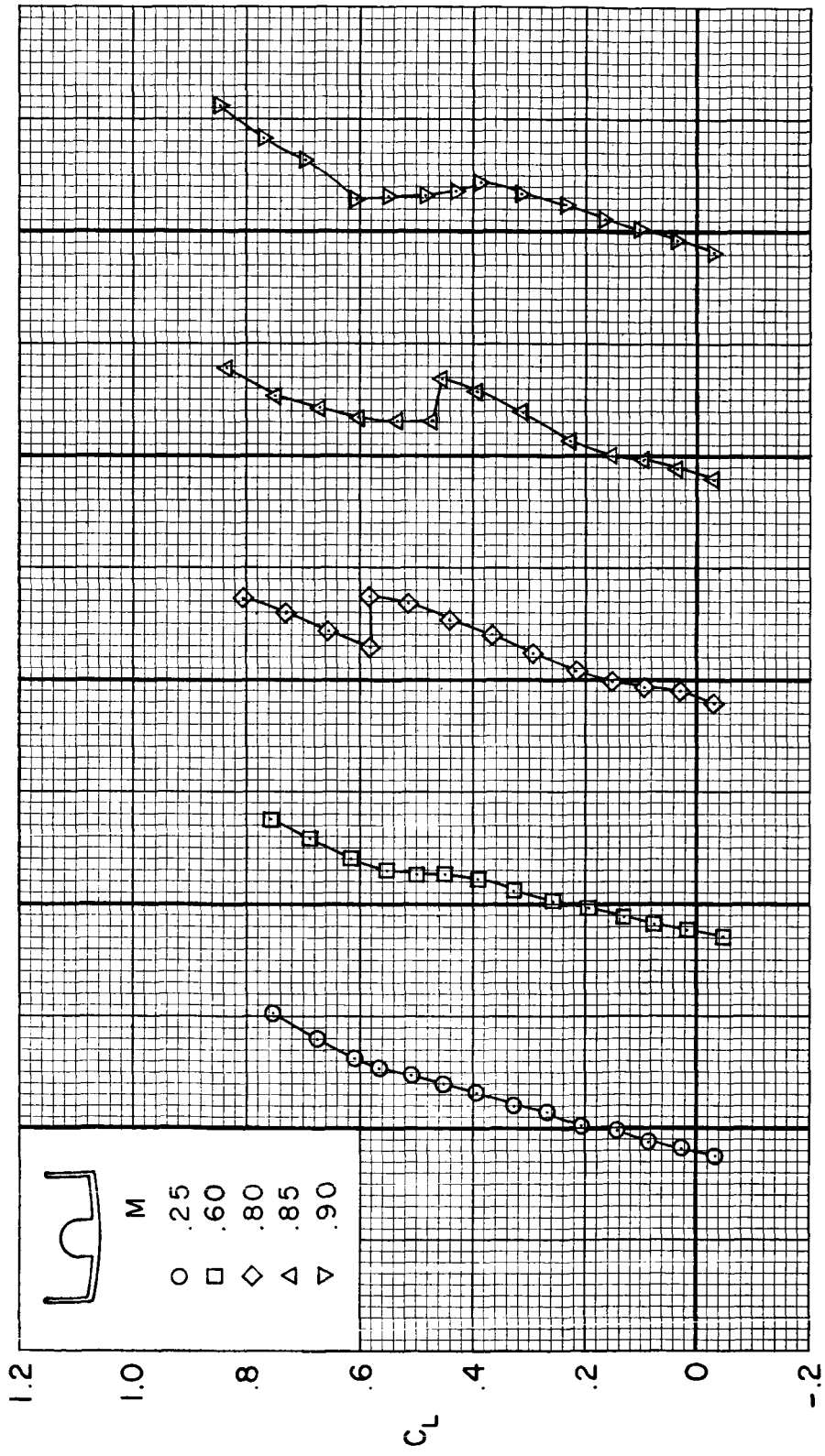

(b) Pitching-moment characteristics.

Figure 32.- Concluded.

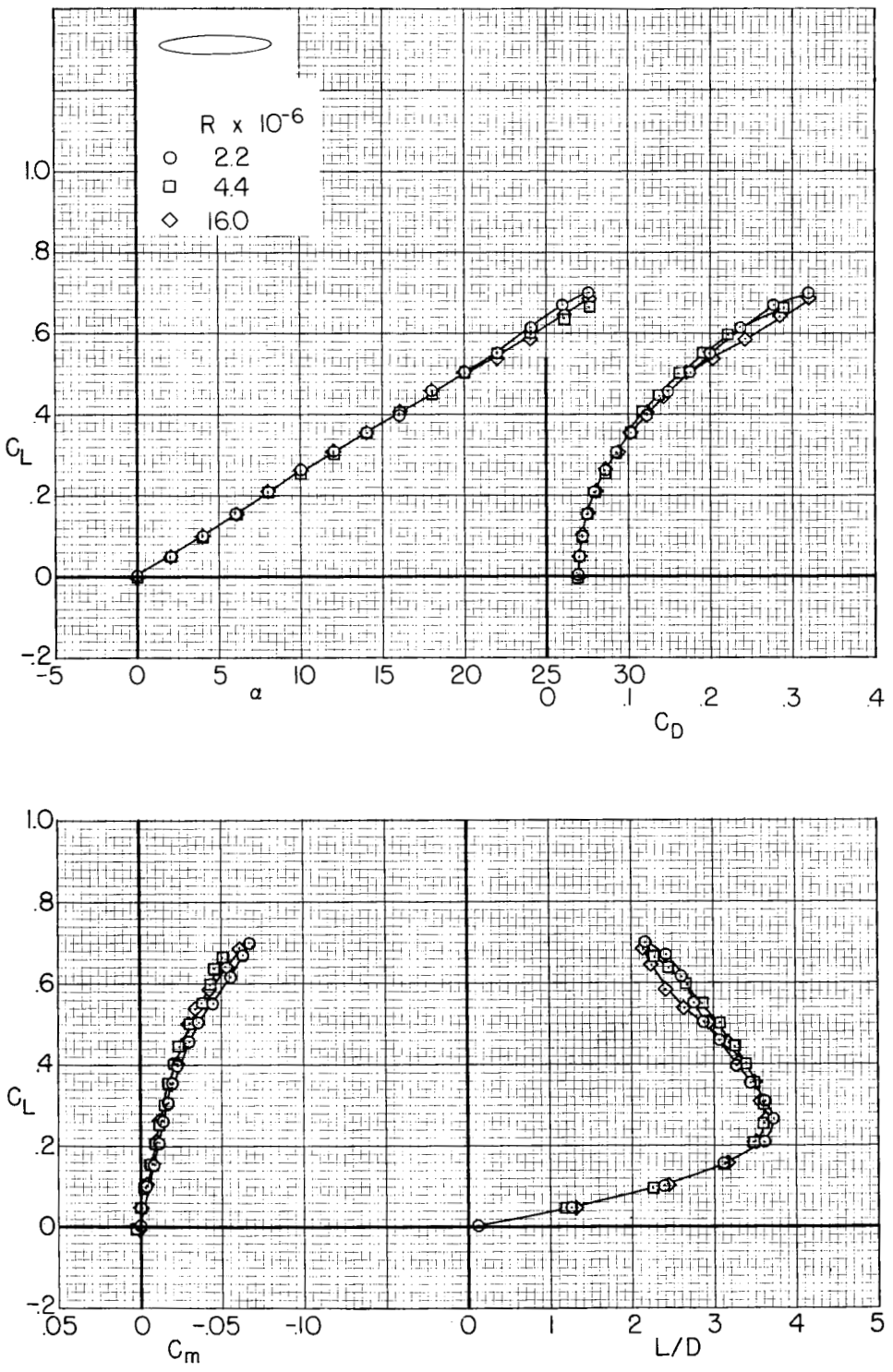

Figure 33.- The effects of Reynolds number on the longitudinal aerodynamic characteristics of model 5; M = 0.25, $\beta = 0^{\circ}$.

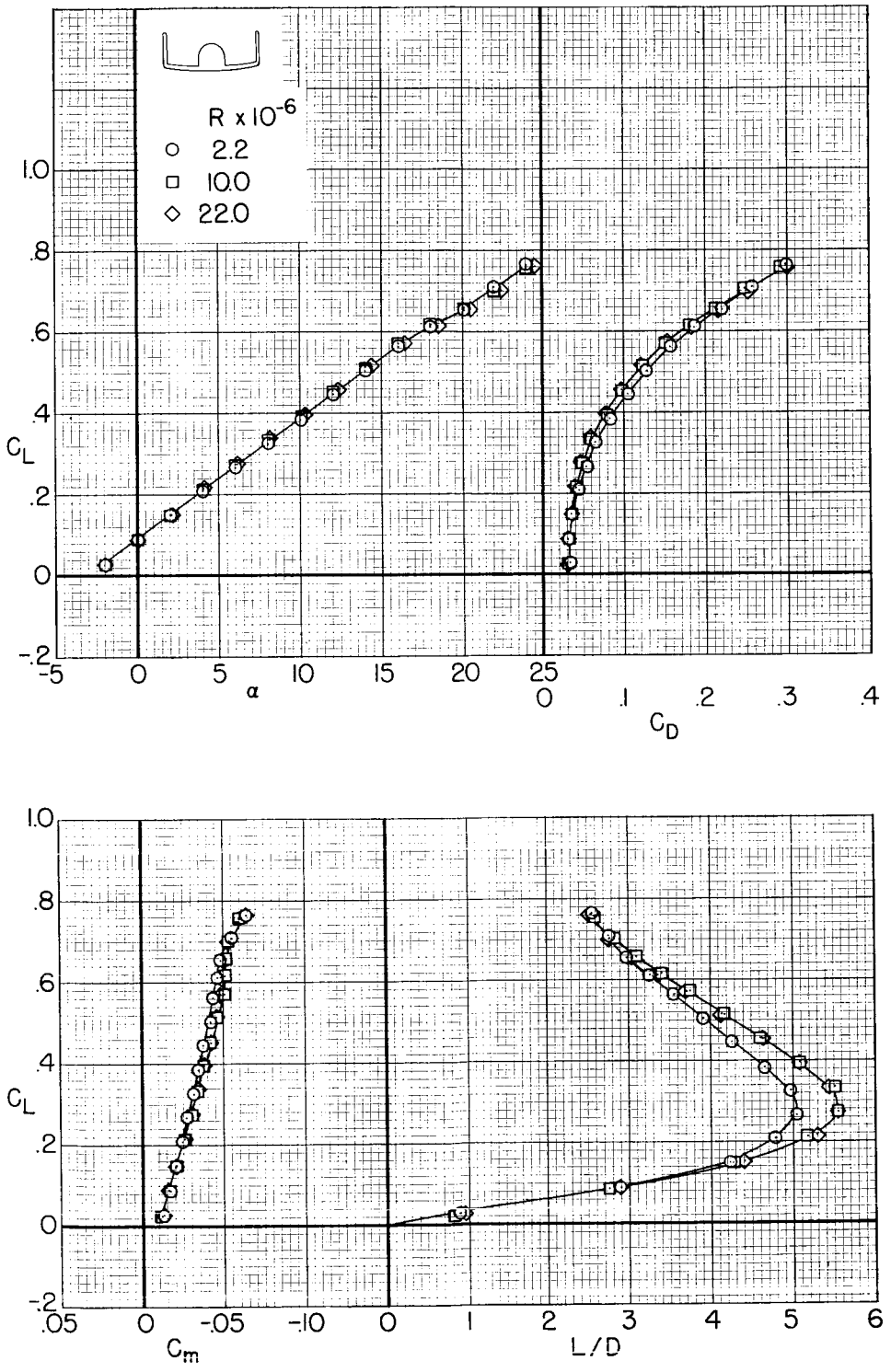

Figure 34.- The effects of Reynolds number on the longitudinal aerodynamic characteristics of model 6 with the small fuselage and vertical surfaces ($\delta_r = 90^\circ$), no elevon controls; M = 0.25, $\beta = 0^\circ$.

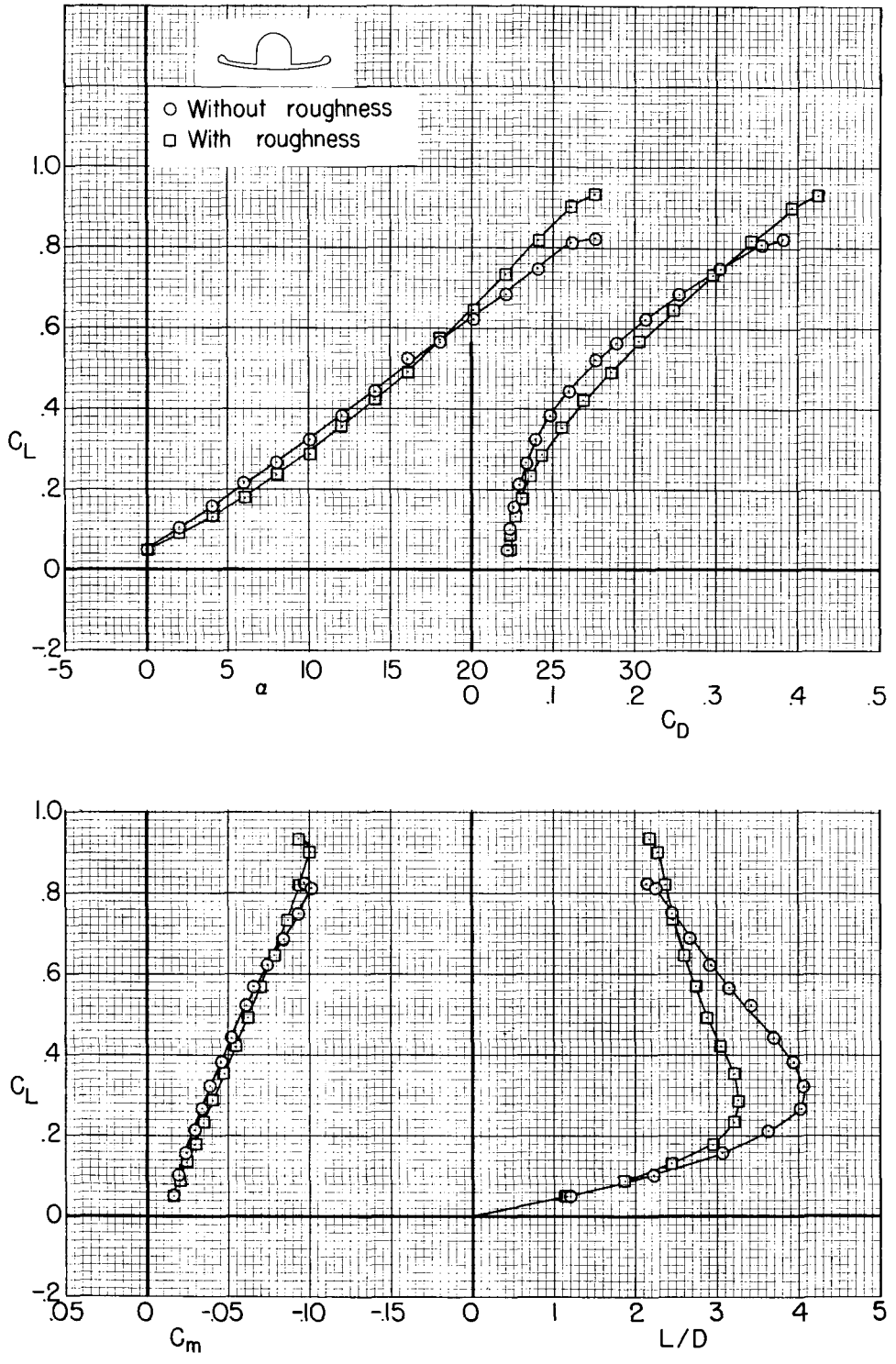

Figure 35.- The effects of leading-edge roughness on the longitudinal aerodynamic characteristics of model 6 with the large fuselage, no elevon controls; M = 0.25, R = 4.4 million, $\beta = 0^{\circ}$.

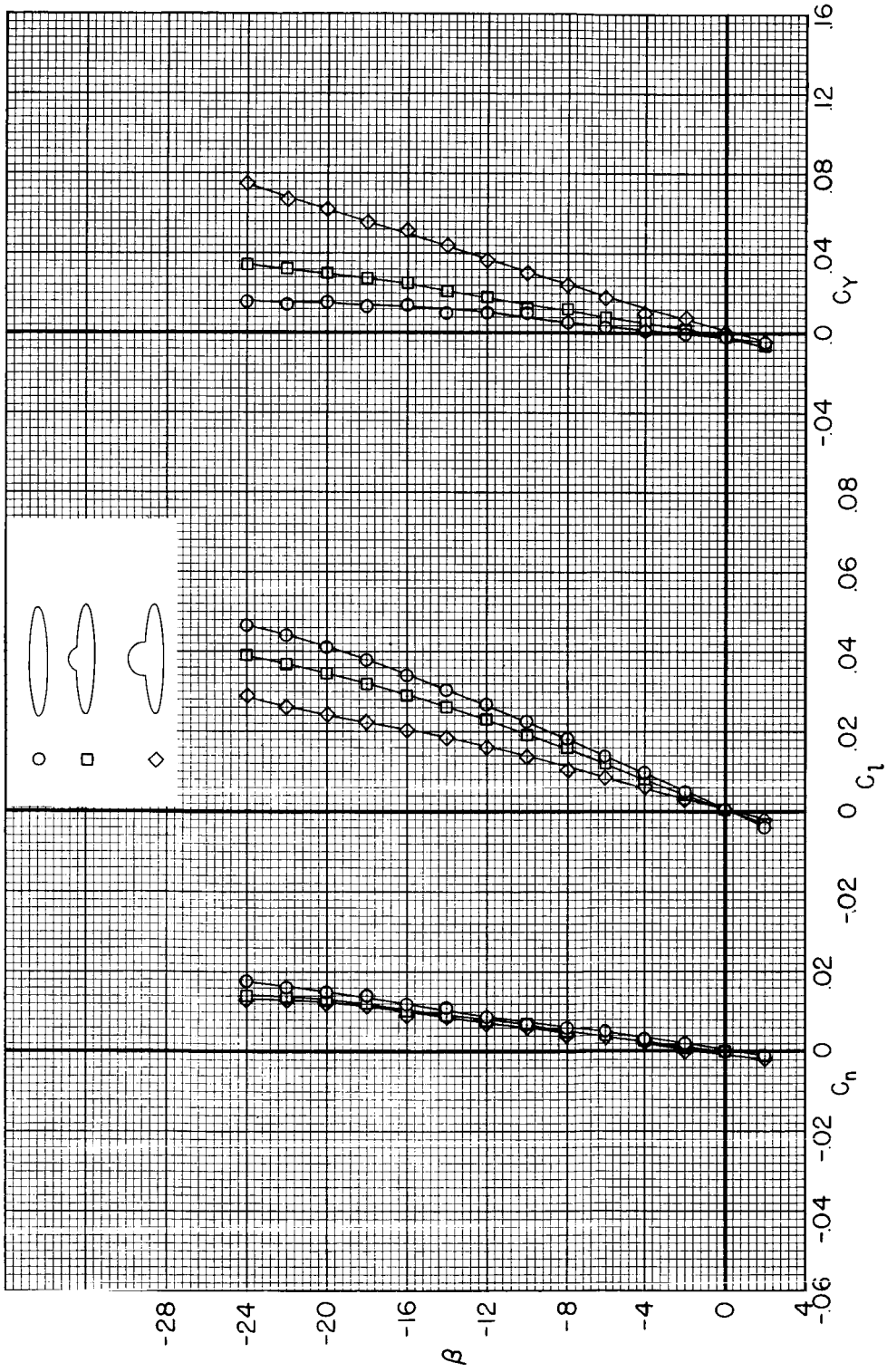

(a) β variable, α = ~9°

Figure 36.- The effects of the fuselage on the lateral and directional characteristics of model 5; M = 0.25, R = 4.4 million.

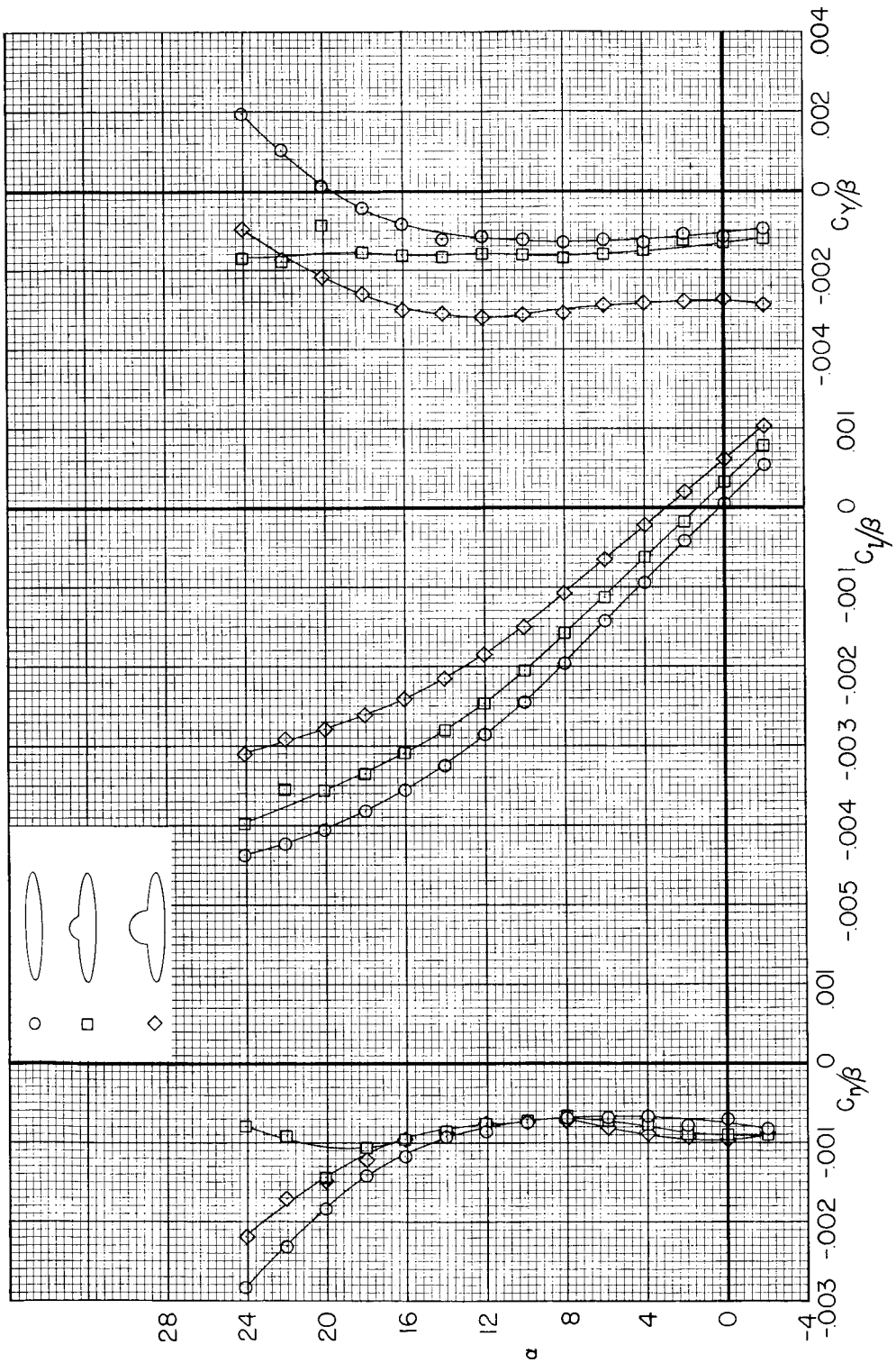

(b) α variable, β = ~9°.

Figure 36.- Concluded.

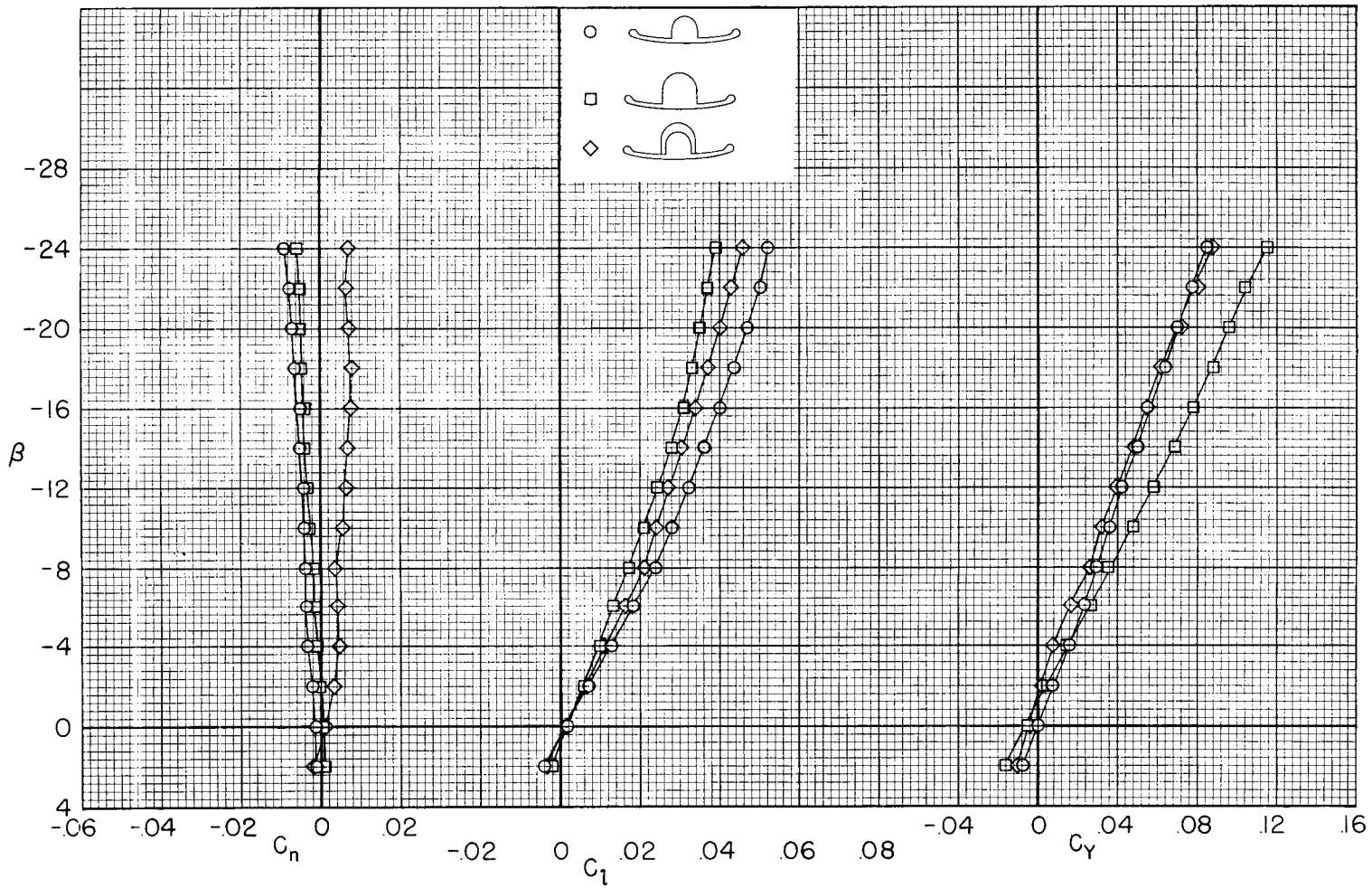

(a) β variable, α = ~9°.

Figure 37.- The effects of fuselage size and shape on the lateral and directional characteristics of model 6; no elevon controls; M = 0.25, R = 4.4 million.

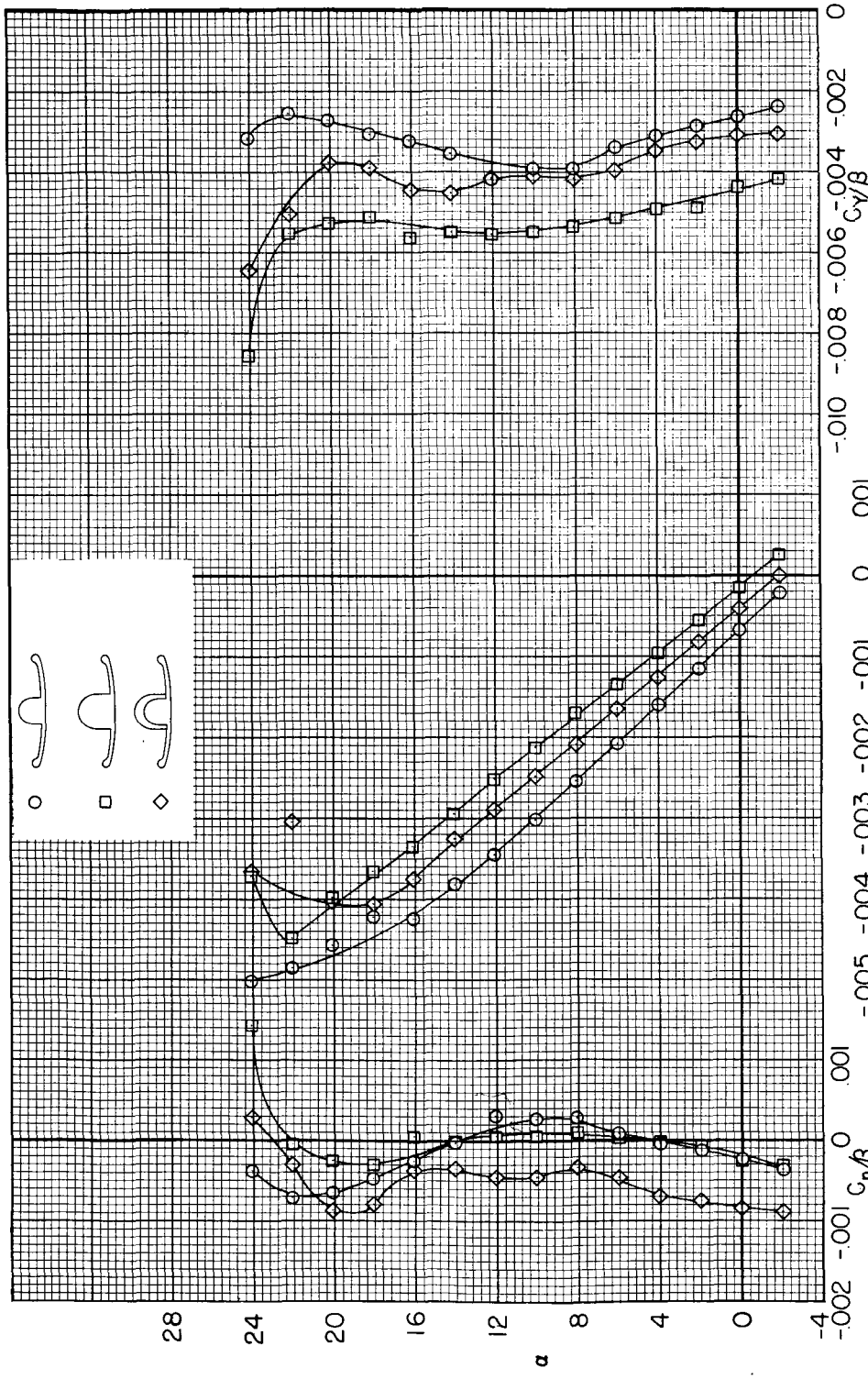

(b) α variable, β = ~9°.

Figure 37.- Concluded.

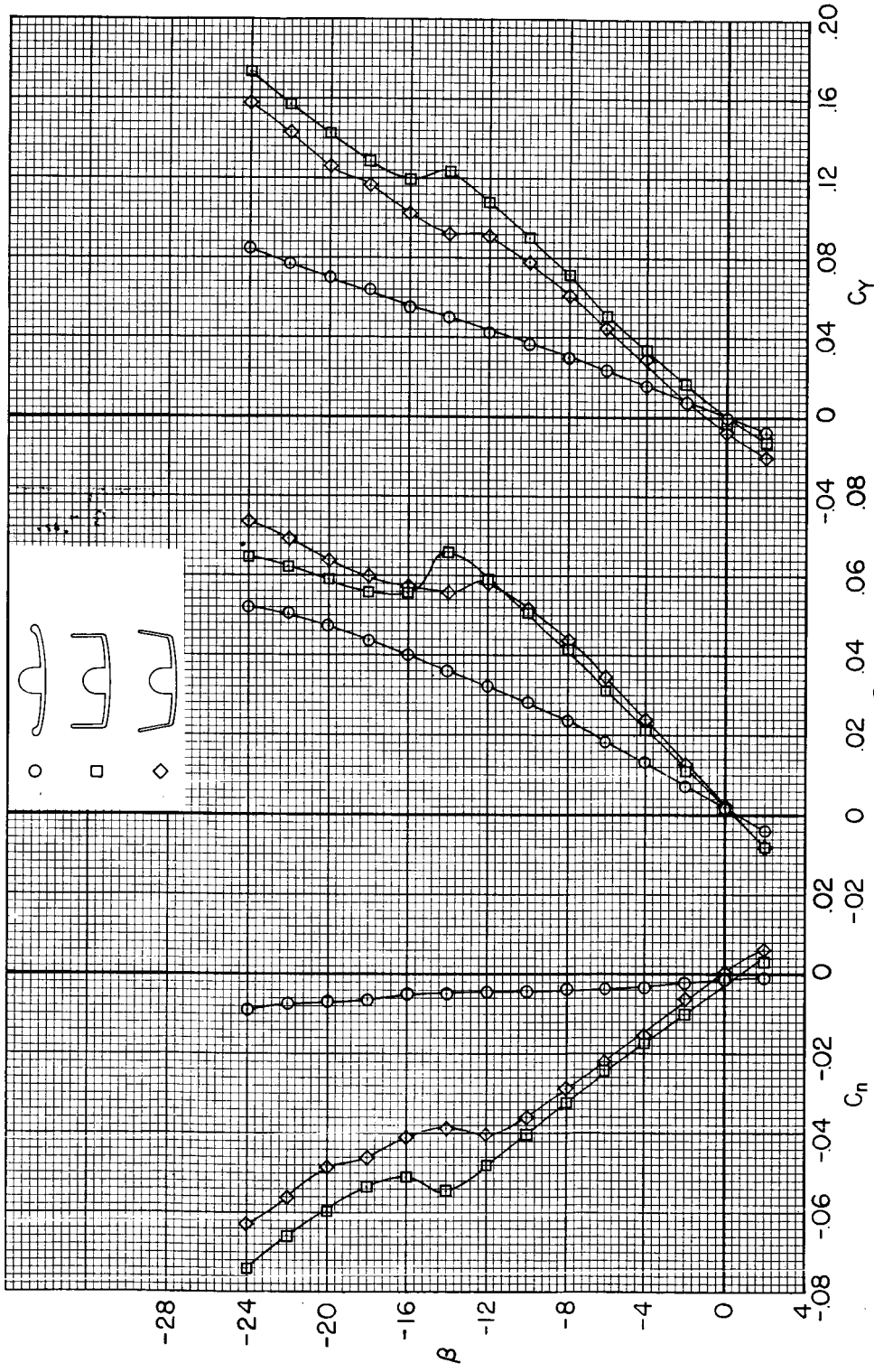

(a) β variable, $\alpha = -9^\circ$.

Figure 38.- The effects of vertical surfaces on the lateral and directional characteristics of model 6 with the small fuselage; no elevon controls; M = 0.25, R = 4.4 million.

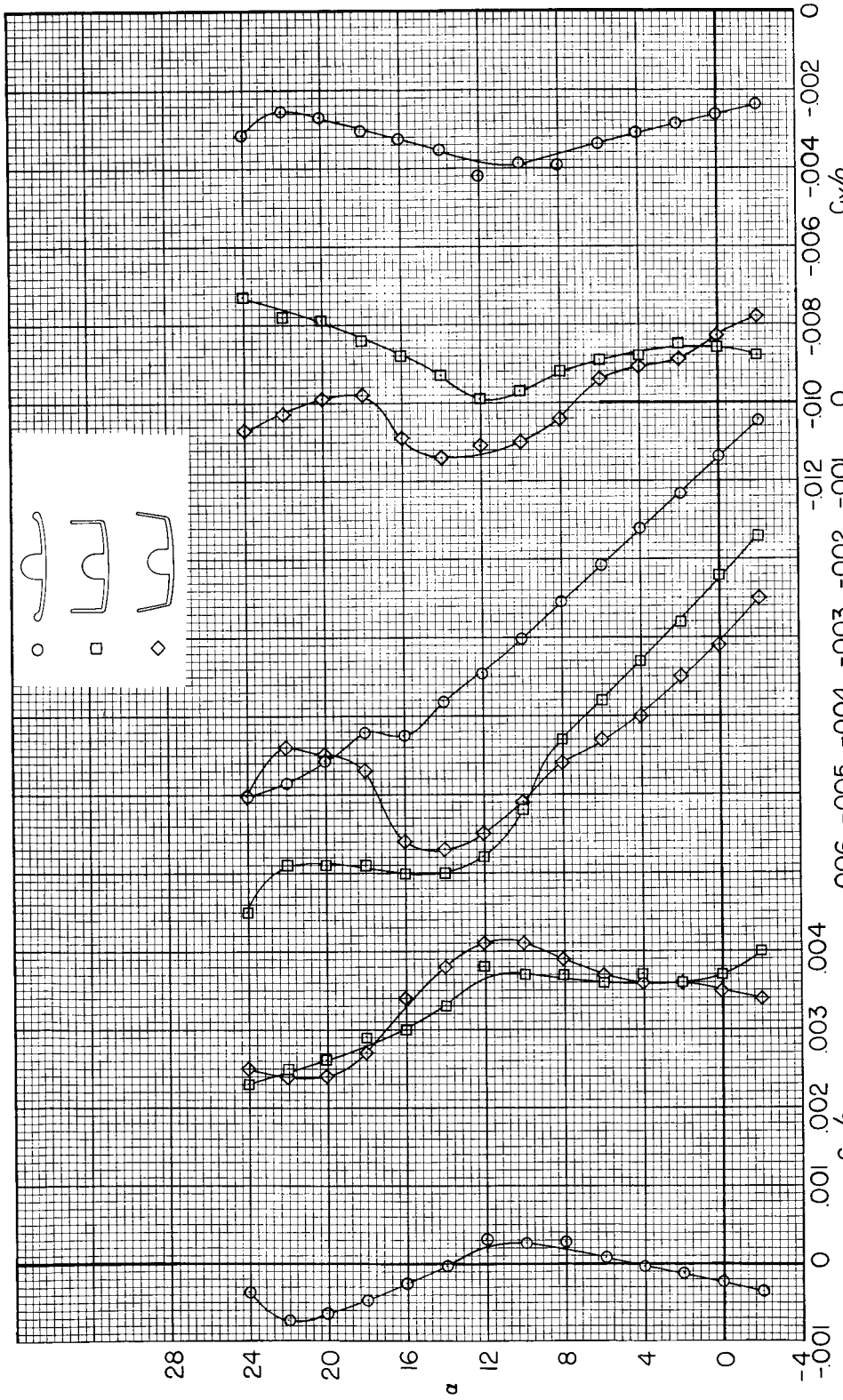

(b) α variable, β = ~9°.

Figure 38.- Concluded.